ASEAN Journal for Science and Engineering in Materials

Journal homepage: https://ejournal.bumipublikasinusantara.id/index.php/ajsem

How to Calculate and Interpret Adsorption Mass Transfer: An Integrated Framework for Kinetics, Diffusion, and Mechanistic Classification with a Practical Example

*Asep Bayu Dani Nandiyanto**

Universitas Pendidikan Indonesia, Bandung, Indonesia
*Correspondence: E-mail: nandiyanto@upi.edu

ABSTRACT

Understanding adsorption mass transfer requires evaluating adsorption kinetics, external-film resistance, intraparticle diffusion, and equilibrium behavior. This study presents an integrated framework for calculating and interpreting adsorption mass transfer using kinetic models, Weber-Morris, Boyd, Fulazzaky, Nandiyanto classification, Furusawa-Smith, and diffusion analysis. An illustrative case is demonstrated to show the calculation procedures, involving ammonium adsorption onto corn-husk particles with different particle sizes and initial concentrations demonstrates. The framework connects concentration changes, adsorption capacity, mass-transfer resistance, mechanistic classification, and effective diffusivity with mechanistic illustrations. This approach provides a practical reference for systematically calculating, comparing, and interpreting adsorption mass-transfer behavior under different operating conditions.

© 2027 Bumi Publikasi Nusantara

ARTICLE INFO

Article History:
Submitted/Received 18 Jul 2026
First Revised 29 Sep 2026
Accepted 14 Oct 2026
First Available online 15 Oct 2026
Publication Date 01 Mar 2027

Keywords:
Adsorption kinetics;
Mass transfer;
Film diffusion;
Intraparticle diffusion;
Effective diffusivity;
Mechanistic classification.

1. INTRODUCTION

Adsorption is widely applied to remove dissolved contaminants from aqueous solutions because of its operational simplicity, effectiveness, and compatibility with various adsorbent materials [1, 2]. However, adsorption performance depends not only on adsorption capacity but also on mass-transfer processes involving bulk-liquid transport, external-film diffusion, intraparticle diffusion, and interactions with adsorption sites [2, 3]. Understanding these processes requires mathematical models that describe adsorption kinetics, diffusion behavior, mass-transfer resistance, and equilibrium progression [2-5]. There are established approaches, for example pseudo-order kinetics, Weber-Morris, and Boyd models, provide complementary information about adsorption rates and transport behavior [2-5]. However, the current models have specific assumptions and limitations, and satisfactory model fitting does not necessarily identify the rate-controlling mass-transfer mechanism [1, 6]. In fact, integrating complementary mathematical models is important for developing a more comprehensive interpretation of adsorption behavior. This study develops an integrated framework for calculating and interpreting adsorption mass transfer. A practical example involving ammonium adsorption onto corn-husk particles is provided to demonstrate calculation procedures, parameter interpretation, and the development of mechanistic illustrations.

2. METHOD

This study employed a calculation-based and illustrative approach to evaluate adsorption mass-transfer behavior. The framework consisted of several stages, including defining the adsorption system, identifying possible adsorption sites and transport pathways, calculating adsorption kinetics, evaluating diffusion and mass-transfer parameters, and integrating the results into mechanistic illustrations. Several mathematical models were incorporated into the framework. Pseudo-first-order (PFO), pseudo-second-order (PSO), and Elovich models were used to describe adsorption kinetics, while Weber-Morris and Boyd models were applied to evaluate diffusion behavior and possible mass-transfer limitations. Furusawa-Smith and Fulazzaky approaches were employed to assess apparent external-film and overall mass-transfer behavior. The Nandiyanto classification was used to categorize mass-transfer progression into early, intermediate, and near-equilibrium stages. Finally, diffusion analysis was conducted to estimate effective diffusivity and characteristic diffusion time. These approaches were integrated to provide a systematic interpretation of adsorption behavior. An illustrative case of ammonium (NH_4^+) adsorption using corn-husk particles with particle sizes of 105, 250, and 500 µm was considered. Initial concentrations ranged from 10 to 80 mg/L, with a solution volume of 300 mL, an adsorbent mass of 3 g, and contact times of 0-150 min. Adsorption capacities were calculated from concentration changes, and the resulting data were used to demonstrate model fitting, parameter calculation, and mechanistic interpretation.

3. RESULTS AND DISCUSSION

3.1. Defining the Adsorption System

The first step in evaluating adsorption mass transfer is to define the adsorption system, including the adsorbate, adsorbent, solution characteristics, and operating conditions. These parameters influence adsorption capacity, transport behavior, and possible adsorption mechanisms. These relationships are schematically presented in **Figure 1**. Smaller particles generally provide shorter diffusion pathways, whereas higher agitation speeds may reduce external-film resistance. Therefore, defining the adsorption system provides a basis for identifying potential transport limitations and constructing mechanistic illustrations (**Table 1**). In short, adsorbate properties such as molecular size, charge, and chemical structure determine possible interactions with the adsorbent. Meanwhile, adsorbent characteristics, including particle size, porosity, surface functional groups, and surface charge, affect the accessibility of adsorption sites and diffusion pathways. Operating conditions, such as initial concentration, pH, temperature, adsorbent dosage, and agitation speed, further influence mass-transfer behavior.

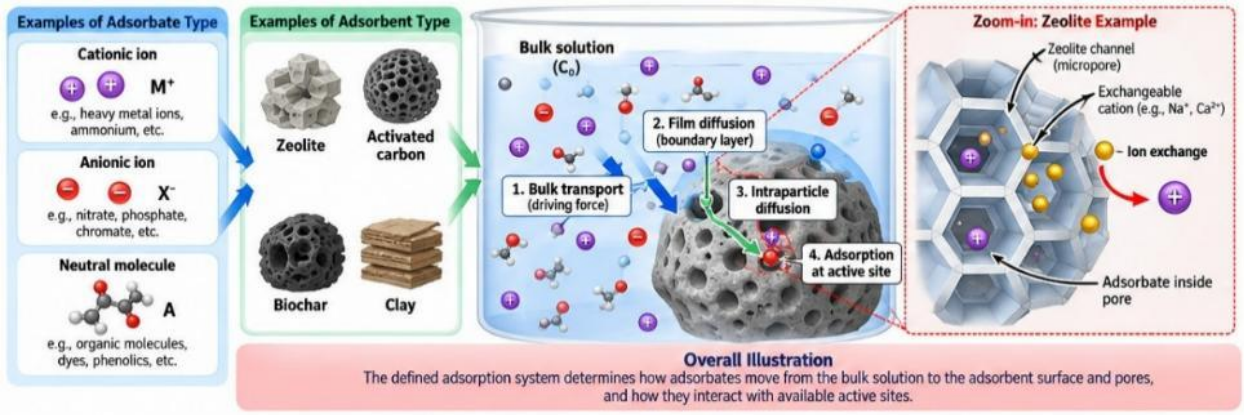


Figure 1. Effects of adsorbate properties, adsorbent characteristics, solution conditions, and operating parameters on adsorption behavior and possible mass-transfer mechanisms.

3.2. Identifying Possible Adsorption Sites

Adsorption occurs at accessible sites located on the external surface or within the internal structure of an adsorbent (**Table 2**). Possible adsorption sites are illustrated in **Figure 2**. In general, possible adsorption sites include external surfaces, pore entrances, internal pore surfaces, functional groups, ion-exchange positions, and specific active sites. Each site contributes differently depending on adsorbate properties and adsorbent characteristics. External surfaces are generally more accessible during the initial adsorption stage, whereas internal sites require adsorbate transport through the pore network. Surface functional groups may promote electrostatic attraction, hydrogen bonding, or other specific interactions. However, the presence of a potential adsorption site does not necessarily indicate its participation in adsorption because accessibility and chemical compatibility must also be considered.

Table 1. Definition of the adsorption system and its expected mechanistic implications.

PARAMETER	POSSIBLE CONDITION / EXAMPLE	EXPECTED IMPACT ON ADSORPTION	IMPLICATION FOR MECHANISTIC ILLUSTRATION
Adsorbate type	Ion	Electrostatic attraction, ion exchange, and competition with other ions may become important	Show charged adsorbates, surface charges, counterions, and possible ion exchange
	Neutral molecule	Adsorption may depend on pore filling, hydrogen bonding, van der Waals forces, or hydrophobic interactions	Show molecular transport into pores and interactions with functional groups
	Organic aromatic molecule	π-π interactions, hydrophobic interactions, and pore filling may contribute	Show interactions between aromatic molecules and carbonaceous surfaces
Adsorbate charge	Cationic	Adsorption may be favored by negatively charged surfaces	Show attraction toward negative surface sites
	Anionic	Adsorption may be favored by positively charged surfaces	Show attraction toward positive surface sites
Adsorbent type	Zeolite	Ion exchange, electrostatic interactions, and pore diffusion may contribute	Show framework channels, exchangeable cations, and ion exchange
	Activated carbon	Surface area, pore filling, and surface functional groups may influence adsorption	Show external surfaces, pores, and pore filling
	Biochar	Heterogeneous surfaces, mineral components, and functional groups may contribute	Show heterogeneous sites, pores, and mineral phases
	Clay	Cation exchange, interlayer adsorption, and electrostatic interactions may occur	Show layered structures and interlayer uptake
Particle size	Small particles	Shorter diffusion pathways and greater external surface area per unit mass may accelerate uptake	Show shorter internal diffusion distances
	Large particles	Longer diffusion pathways may increase intraparticle resistance	Show longer internal transport pathways
Porosity	Highly porous	Greater accessible internal surface area; potential intraparticle diffusion limitations	Show adsorption within internal pores
	Low porosity	Adsorption may occur predominantly near external surfaces	Emphasize surface adsorption
Surface functional groups	-OH, -COOH, $-NH_2$, etc.	May promote hydrogen bonding, complexation, acid-base interactions, or electrostatic attraction	Show interactions with functional groups
Surface charge	Negative	May promote cation adsorption	Show cations approaching negatively charged surfaces
	Positive	May promote anion adsorption	Show anions approaching positively charged surfaces

Table 1 (continued). Definition of the adsorption system and its expected mechanistic implications.

PARAMETER	POSSIBLE CONDITION / EXAMPLE	EXPECTED IMPACT ON ADSORPTION	IMPLICATION FOR MECHANISTIC ILLUSTRATION
Solution pH	Below pH_pzc	Surface charge tends to become more positive	Illustrate pH-dependent electrostatic interactions
	Above pH_pzc	Surface charge tends to become more negative	Illustrate attraction of cationic adsorbates
Initial concentration	Low	Lower surface coverage and reduced competition among adsorbates	Show relatively few adsorbate molecules
	High	Greater concentration driving force and potentially faster site occupation	Show greater surface coverage
Adsorbent dosage	Low	Fewer available adsorption sites per solution volume	Show greater competition for adsorption sites
	High	More adsorption sites available per solution volume	Show more accessible sites
Agitation speed	Low	Thicker effective liquid boundary layer and potentially greater external-film resistance	Show a thicker boundary layer
	High	Reduced external-film resistance under stronger mixing	Show a thinner boundary layer
Temperature	Increasing	May enhance diffusion; equilibrium capacity may increase or decrease	Show faster diffusion where relevant
Competing species	Other ions or molecules	Competition may reduce target-adsorbate uptake	Show competing species approaching adsorption sites

Table 2. Possible adsorption sites, their characteristics, and mechanistic implications.

ADSORPTION SITE	TYPICAL CHARACTERISTICS	POSSIBLE ADSORPTION BEHAVIOR	IMPLICATION FOR ILLUSTRATION
External surface	Easily accessible outer particle surface	Rapid initial adsorption	Show adsorbates occupying external sites
Pore entrance	Opening connecting external and internal regions	Controls access to internal adsorption sites	Show adsorbate entering pores
Internal pore surface	Micropores, mesopores, or macropores	Intraparticle diffusion followed by adsorption	Show diffusion and adsorption along internal pore walls
Surface functional groups	-OH, -COOH, $-NH_2$, -C=O, etc.	Hydrogen bonding, electrostatic interactions, or complexation	Show adsorbate interacting with chemical groups
Ion-exchange sites	Exchangeable ions associated with the solid structure	Replacement of exchangeable ions by adsorbate ions	Show ion-exchange processes
Specific active sites	Defects, metal centers, edges, or mineral phases	Strong or selective adsorption	Highlight localized high-affinity sites

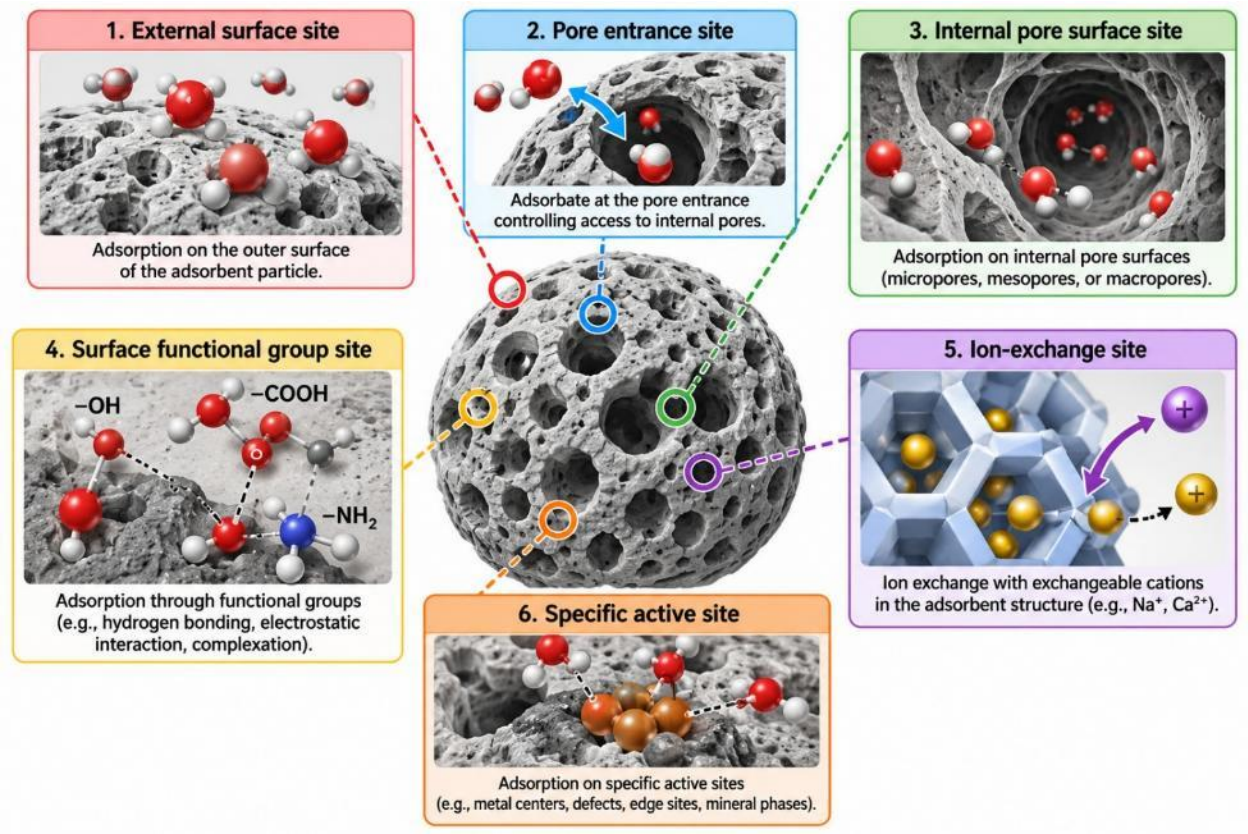


Figure 2. Schematic representation of possible adsorption sites: (1) external surfaces, (2) pore entrances, (3) internal pore surfaces, (4) functional groups, (5) ion-exchange sites, and (6) specific active sites.

3.3. Understanding Time-Dependent Adsorption Behavior

Adsorption behavior can initially be evaluated from changes in residual adsorbate concentration (C_t) with contact time (t) (**Table 3**). These concentration profiles are illustrated in **Figure 3.** A typical adsorption profile exhibits rapid initial concentration decrease, gradual concentration decrease, and apparent equilibrium. The initial stage is commonly associated with a relatively large concentration gradient and accessible adsorption sites, whereas the subsequent decrease in adsorption rate reflects the progressive approach toward equilibrium.

In addition, there is a possible concentration increase after apparent stabilization. Such an increase should not automatically be interpreted as desorption because other physical, chemical, and experimental factors may also contribute. The possible causes of increasing residual concentration are summarized in **Table 4**. These include desorption, redistribution between adsorption sites, dissolution or leaching, changes in solution chemistry, mixing and sampling effects, and analytical uncertainty.

Table 3. Time-dependent concentration profiles and possible mechanistic interpretations.

CONCENTRATION BEHAVIOR	TYPICAL PROFILE	POSSIBLE INTERPRETATION	IMPLICATION FOR ILLUSTRATION
Rapid concentration decrease	C_t decreases sharply from C_0	Rapid initial uptake associated with a large concentration gradient and accessible sites	Show rapid transport toward the adsorbent
Gradual concentration decrease	C_t continues decreasing at a slower rate	Progressive adsorption and decreasing net uptake rate	Show gradual occupation of accessible sites
Stable concentration	C_t approaches a nearly constant value	Adsorption approaches apparent equilibrium	Show nearly stable distributions between solution and adsorbent
Concentration increase after stabilization	C_t increases after a minimum or plateau	Possible desorption, solution-chemistry changes, leaching, or experimental effects	Show possible release of adsorbates or changes in solution concentration

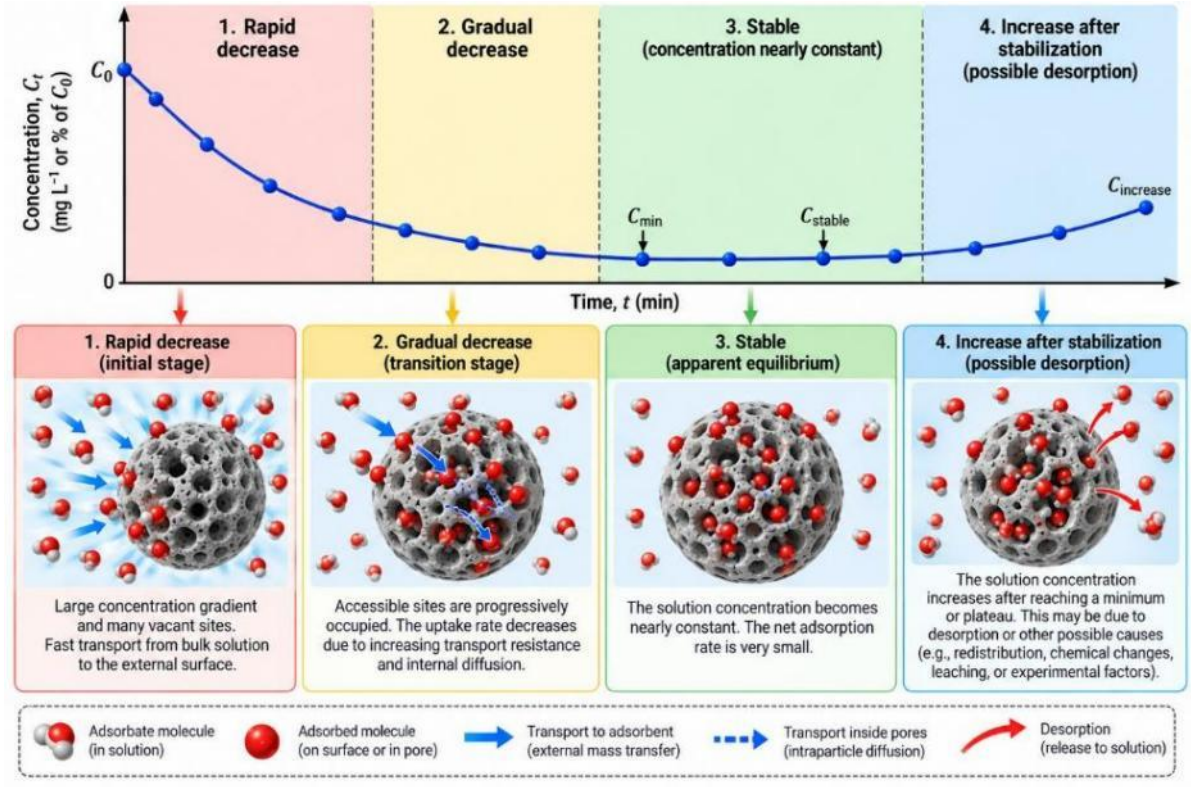
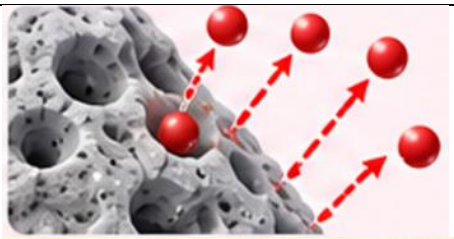
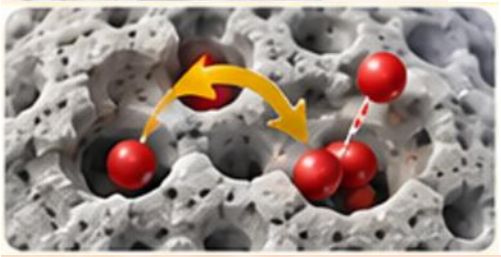
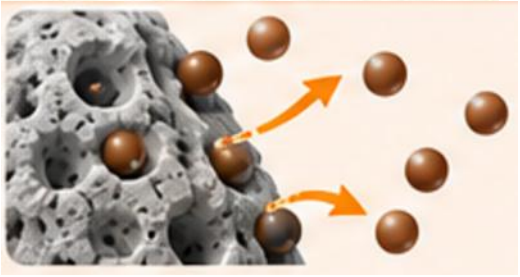


Figure 3. Schematic representation of time-dependent adsorbate concentration, showing rapid concentration decrease, gradual decrease, apparent equilibrium, and possible concentration increase after stabilization.

The relationship between concentration gradients and adsorption transport is further illustrated in **Figure 4**. Adsorbate species move from the bulk solution across the external liquid film toward the adsorbent surface and subsequently migrate into accessible pores. These processes contribute to the time-dependent concentration changes observed during adsorption.

Table 4. Factors contributing to increasing adsorbate concentration after equilibrium.

FACTOR	EXPLANATION	ILLUSTRATION
Desorption.	Weakly adsorbed species may be released back into the solution	
Redistribution between adsorption sites	Adsorbate may move from one region or site to another, changing the measured concentration in solution	
Dissolution or leaching	Species released from the adsorbent may increase the measured concentration	
Changes in solution chemistry	Variations in pH, ionic strength, or adsorbate speciation may shift the adsorption-desorption balance	
Mixing and sampling effects	Incomplete mixing or non-representative sampling can produce an apparent increase in concentration	
Analytical uncertainty	Instrumental error, calibration variation, or measurement noise may also cause fluctuations in the measured concentration	

3.4. Identifying Mass-Transfer Pathways

The adsorption mass-transfer pathway describes the movement of adsorbate species from the bulk solution toward accessible adsorption sites. As summarized in **Table 5**, this pathway involves bulk-liquid transport, external-film diffusion, arrival at the adsorbent surface, intraparticle diffusion, and transport toward active sites. The relative contribution of these processes depends on particle size, porosity, agitation speed, and concentration gradients.

These transport processes are schematically illustrated in **Figure 5**. External-film diffusion involves adsorbate movement across the liquid boundary layer, whereas intraparticle diffusion describes migration through pores and internal regions. Although these processes may occur simultaneously, identifying the transport pathway does not necessarily establish which process controls the overall adsorption rate.

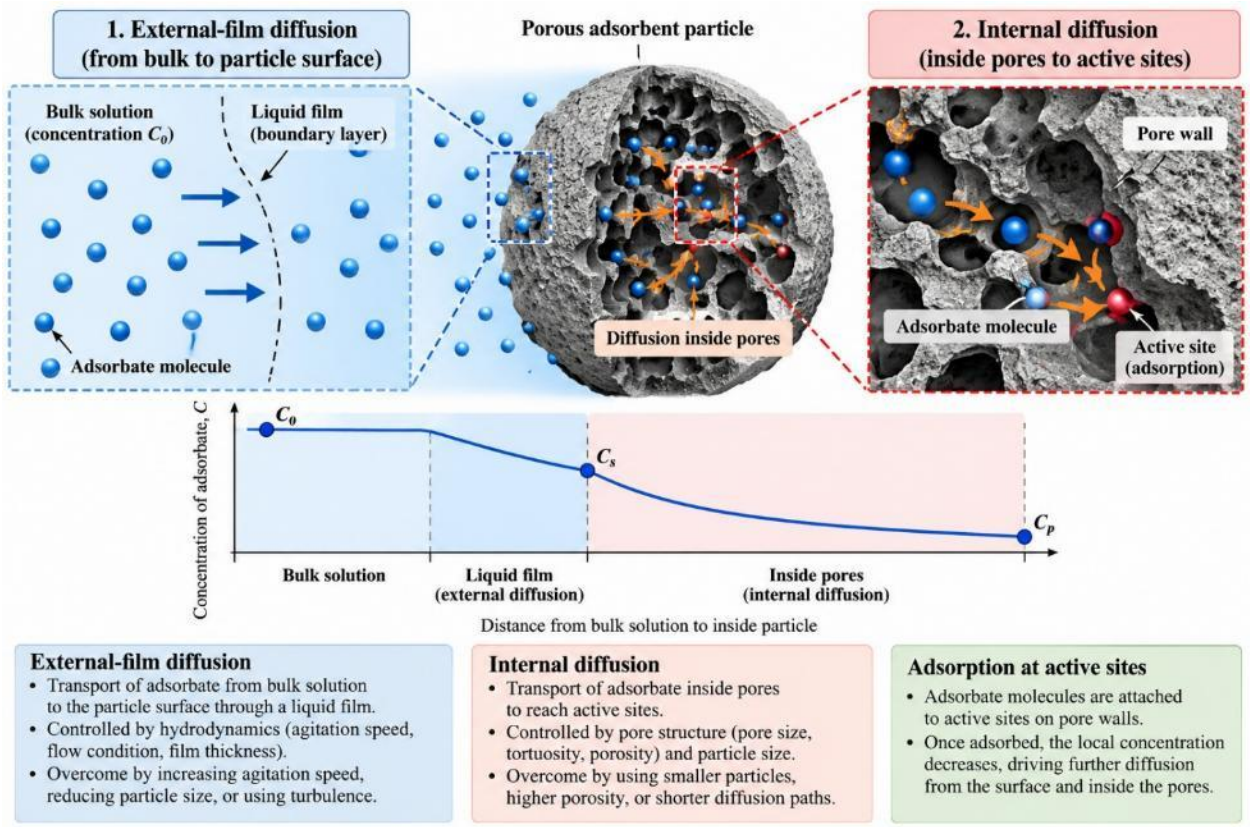


Figure 4. Schematic illustration of external-film diffusion and internal diffusion during adsorption, showing concentration gradients from the bulk solution toward the adsorbent surface and pore interior.

Table 5. Possible mass-transfer pathways during adsorption and their mechanistic interpretations.

MASS-TRANSFER REGION	MAIN PROCESS	POSSIBLE INDICATION	IMPLICATION FOR ILLUSTRATION
Bulk solution transport	Adsorbate moves through the bulk liquid toward the adsorbent	Concentration gradient provides a driving force	Show adsorbates moving toward the particle
Film diffusion	Adsorbate crosses the liquid boundary layer surrounding the adsorbent	Sensitivity to agitation and hydrodynamic conditions	Show the liquid-film boundary layer
External surface arrival	Adsorbate reaches accessible sites on the outer particle surface	Rapid initial uptake may occur	Show adsorption at external sites
Intraparticle diffusion	Adsorbate migrates through pores toward internal regions	Sensitivity to particle size, pore structure, and diffusion distance	Show migration through internal pores
Transport to active sites	Adsorbate reaches specific adsorption locations	Depends on site accessibility and local interactions	Show adsorption at internal or external active sites

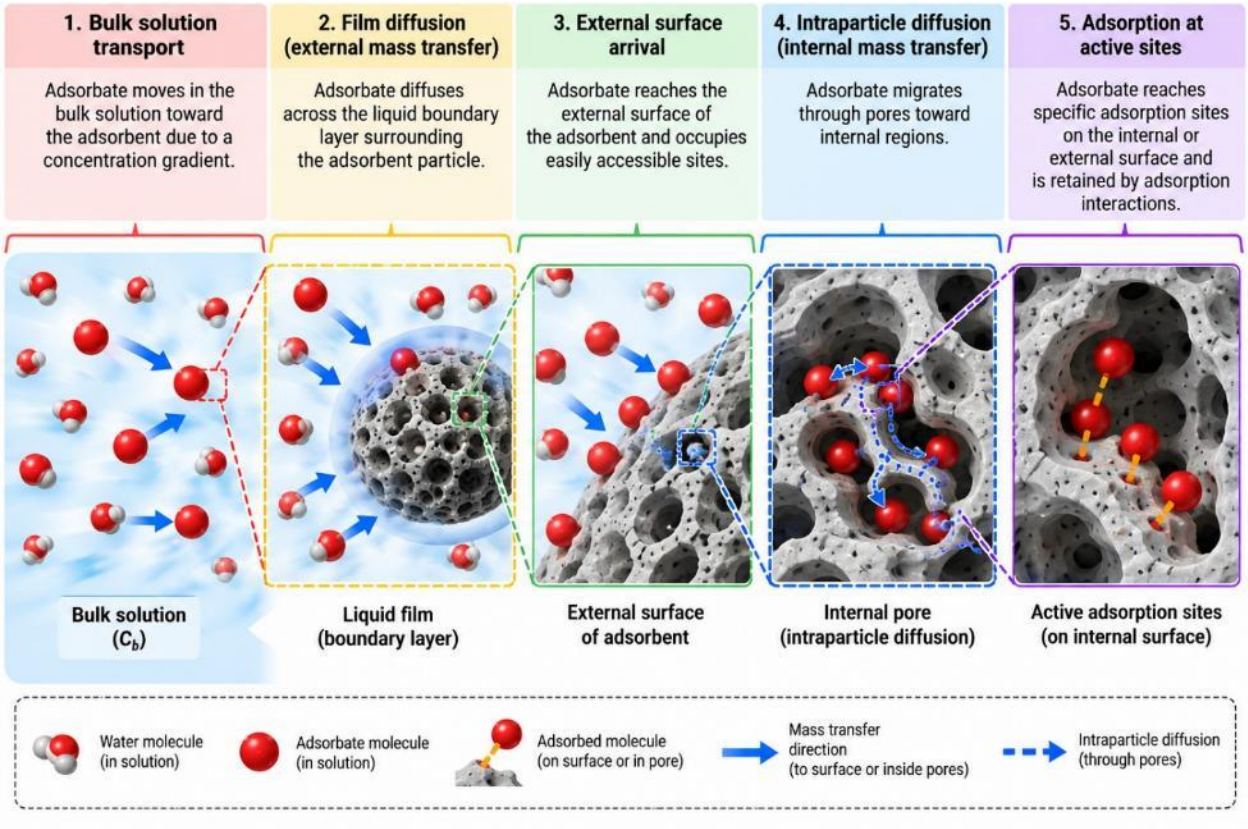


Figure 5. Schematic representation of adsorption mass-transfer pathways, including bulk-liquid transport, external-film diffusion, surface arrival, intraparticle diffusion, and transport toward active adsorption sites.

3.5. Determining the Rate-Controlling Mass-Transfer Step

The overall adsorption rate may be influenced by external-film resistance, intraparticle diffusion, or their combined contributions. Therefore, identifying the rate-controlling step requires complementary mathematical approaches. As summarized in **Table 6**, Weber-Morris analysis identifies apparent multistage diffusion behavior, whereas the Boyd model evaluates whether adsorption is consistent with predominant intraparticle diffusion or additional external-film resistance. Furusawa-Smith analysis estimates apparent external mass-transfer behavior, while the Fulazzaky approach evaluates external-film, global, and internal-derived mass-transfer factors. The Nandiyanto classification categorizes mass-transfer progression, whereas effective diffusivity analysis estimates characteristic internal transport parameters.

The integration of these approaches is illustrated in **Figure 6**. Combining kinetic models, diffusion analysis, mass-transfer factors, and operating-variable effects provides a broader interpretation than applying individual models independently. However, model fitting alone does not definitively identify a controlling mechanism without supporting experimental evidence.

The principal mathematical equations used in this framework are summarized in **Table 7**. These equations include adsorption-capacity calculations, Weber-Morris and Boyd transformations, Furusawa-Smith and Fulazzaky analyses, the Nandiyanto classification, and diffusion-related parameters.

3.6. Practical Example: Adsorption Mass-Transfer Calculations

To demonstrate the application of the integrated framework, an illustrative adsorption case involving ammonium (NH_4^+) removal using corn-husk particles was analyzed. The calculation procedure includes adsorption kinetics, Weber-Morris, Boyd, Furusawa-Smith, Fulazzaky, Nandiyanto classification, and effective diffusivity analysis. Each approach provides complementary information regarding adsorption rates, mass-transfer resistance, diffusion behavior, and mechanistic interpretation. The calculations were performed using concentration-time data to illustrate how mathematical models can be applied systematically to understand adsorption mass transfer.

Table 6. Mathematical and experimental approaches for evaluating adsorption mass-transfer mechanisms and their interpretations.

APPROACH	MAIN INFORMATION OBTAINED	POSSIBLE INTERPRETATION	ILLUSTRATION IMPLICATION
Weber-Morris model	Identifies apparent intraparticle-diffusion regions from (q_t) versus ($t^{½}$)	Multiple linear regions may indicate changes in transport behavior; a nonzero intercept suggests that intraparticle diffusion is not the only contribution	Illustrate initial, intermediate, and late uptake stages
Boyd model	Evaluates whether uptake is consistent with predominant intraparticle diffusion	A regression passing approximately through the origin supports intraparticle-diffusion control under model assumptions; a nonzero intercept suggests additional resistance	Compare liquid-film and intraparticle transport
Furusawa-Smith analysis	Estimates apparent external mass-transfer behavior	A larger apparent external mass-transfer coefficient indicates faster initial transport under comparable conditions	Illustrate transport across the external liquid film
Fulazzaky model	Evaluates external-film, global, and internal-derived mass-transfer factors	Describes apparent contributions to mass-transfer behavior over contact time	Illustrate changes in external-film and overall transfer factors
Nandiyanto classification	Classifies adsorption progression using a mass-transfer progress index and transition parameters	Distinguishes early, intermediate, and near-equilibrium stages according to defined classification thresholds	Illustrate transitions between adsorption stages
Effective diffusivity analysis	Estimates effective diffusivity and characteristic diffusion time	Larger effective diffusivity generally indicates faster internal transport under comparable model assumptions	Compare characteristic diffusion times for different particle sizes
Particle-size effect	Evaluates the relationship between particle size and transport behavior	Faster uptake by smaller particles may be consistent with shorter diffusion distances	Show differences in internal transport distance
Agitation-speed effect	Evaluates the influence of mixing on external-film transport	Strong agitation dependence may indicate an important external-film contribution	Compare thick and thin effective liquid-film layers

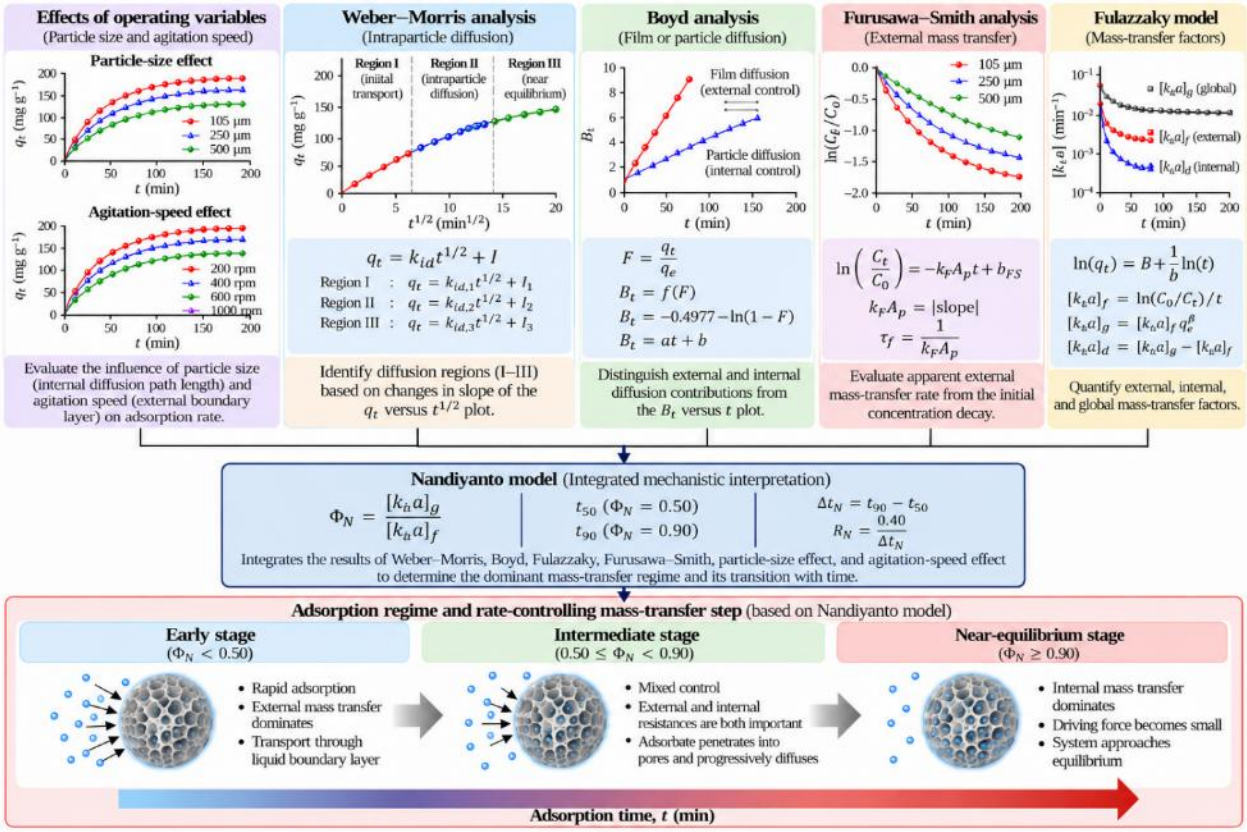


Figure 6. Integrated framework for interpreting adsorption kinetics, external-film resistance, intraparticle diffusion, mass-transfer classification, and effective diffusivity.

Table 7. Main equations for calculating adsorption capacity, diffusion behavior, mass-transfer parameters, and mechanistic classification.

NO	CALCULATION/ MODEL	EQUATION	MAIN PARAMETER	PURPOSE
1	Normalized concentration	$C^* = C_t/C_0$	C^*	Determines the fraction of adsorbate remaining in solution
2	Adsorption capacity	$q_t = \frac{(C_0 - C_t)V}{m}$	q_t	Calculates adsorption capacity at time *t*
3	Equilibrium adsorption capacity	$q_e = \frac{(C_0 - C_e)V}{m}$	q_e	Calculates adsorption capacity at equilibrium
4	Removal efficiency	$R = \frac{C_0 - C_t}{C_0} \times 100\%$	R	Determines adsorbate removal efficiency
5	Adsorption kinetics			
	Pseudo-first-order (PFO)	$ln(q_e\text{-}q_t) = ln(q_e) - k_1.t$	k_1, q_e	Evaluates apparent first-order adsorption kinetics
	Pseudo-second-order (PSO)	$\frac{t}{q_t} = \frac{1}{k_2 q_e^2} + \frac{t}{q_e}$	k_2, q_e	Evaluates apparent second-order adsorption kinetics
	Elovich model	$q_t = \frac{1}{\beta} ln(\alpha\beta) + \frac{1}{\beta} ln\, t$	α, β	Evaluates adsorption kinetics with a changing apparent uptake rate

Table 7 (continued). Main equations for calculating adsorption capacity, diffusion behavior, mass-transfer parameters, and mechanistic classification.

NO	CALCULATION/ MODEL	EQUATION	MAIN PARAMETER	PURPOSE
6	Weber-Morris model, Intraparticle diffusion	$q_t = kid.t^{½} + I$	k_{id},I	Identifies apparent diffusion stages and boundary-layer contributions
7	Boyd model, Fractional adsorption	$F= q_t/q_e$	F	Calculates fractional adsorption uptake
	Boyd function, $F < 0.85$	$B_t = \left[\sqrt{\pi} - \sqrt{\pi - \frac{\pi^2 F}{3}}\right]^2$	B_t	Transforms fractional uptake at lower adsorption fractions
	Boyd function, $F > 0.85$	$B_t = -0.4977 - ln(1 - F)$	B_t	Transforms fractional uptake near equilibrium
	Boyd regression	$Bt = a.t + b$	a,b	Evaluates deviation from ideal intraparticle-diffusion control
8	Fulazzaky analysis	$ln\, q_t = B + \frac{1}{\beta} ln\, t$	B,β	Determines regression parameters for mass-transfer analysis
	External-film mass-transfer factor	$[k_L a]_f = \frac{ln(C_0/C_t)}{t}$	$[k_L a]_f$	Evaluates apparent external-film transfer
	Global mass-transfer factor	$[k_L a]_g = [k_L a]_f q_t^{\beta}$	$[k_L a]_g$	Calculates the global mass-transfer factor using the manuscript formulation
	Internal-derived mass-transfer term	$[k_L a]_d = [k_L a]_g - [k_L a]_f$	$[k_L a]_d$	Calculates the difference between global and external-film factors
9	Nandiyanto classification			
	Mass-transfer progress index	$\Phi_N = \frac{[k_L a]_g}{[k_L a]_f}$	Φ_N	Calculates the classification index
	Early stage	$\Phi_N < 0.50$	Φ_N	Identifies the early stage
	Intermediate stage	$0.50 \leq \Phi_N < 0.90$	Φ_N	Identifies the intermediate stage
	Near-equilibrium stage	$\Phi_N \geq 0.90$	Φ_N	Identifies the operational near-equilibrium stage
	Transition times	$\Phi_N\,(t_{50}) = 0.50;\ \Phi_N\,(t_{90}) = 0.90$	t_{50},t_{90}	Determines characteristic transition times
	Intermediate-stage duration	$\Delta t_N = t_{90} - t_{50}$	Δt_N	Determines the intermediate-stage duration
	Transition rate	$R_N = 0.40 / \Delta t_N$	R_N	Quantifies progression between classification thresholds
10	Furusawa-Smith analysis, External mass-transfer regression	$ln(C_t/C_0) = -k_f A_p t + b$	$k_f.A_p$,b	Estimates apparent external mass-transfer behavior
	Characteristic external-transfer time	$\tau_f = \frac{1}{k_f A_p}$	τ_f	Estimates characteristic external-transfer time

Table 7 (continued). Main equations for calculating adsorption capacity, diffusion behavior, mass-transfer parameters, and mechanistic classification.

NO	CALCULATION/ MODEL	EQUATION	MAIN PARAMETER	PURPOSE
11	Effective diffusivity analysis, Diffusion model	$ln(1-F) = ln\left(\frac{6}{\pi^2}\right) - \frac{\pi^2 D_e t}{R_p^2}$	D_e	Describes the long-time approximation for spherical-particle diffusion
	Linear regression	$ln(1-F) = at + b$	a,b	Determines the apparent diffusion slope
	Effective diffusivity	$D_e = -\frac{aR_p^2}{\pi^2}$	D_e	Estimates effective diffusivity
	Characteristic diffusion time	$\tau_d = \frac{R_p^2}{D_e}$	τ_d	Estimates characteristic diffusion time

Note: C_0, C_t, and C_e are initial, time-dependent, and equilibrium concentrations (mg/L); V is solution volume (L); m is adsorbent mass (g); q_t and q_e are adsorption capacities (mg/g); t is contact time (min); k_1 and k_2 are PFO and PSO rate constants; α and β are Elovich parameters; k_{id} and I are Weber-Morris parameters; F is fractional uptake; B_t is the Boyd function; $k_f.A_p$ is an apparent external mass-transfer rate coefficient; $[k_La]_f$, $[k_La]_g$, and $[k_La]_d$ are the Fulazzaky factors; Φ_N is the Nandiyanto classification index; D_e is effective diffusivity (m^2/s); R_p is particle radius (m); and τ_d is characteristic diffusion time. Time units must be consistent in diffusivity calculations.

3.6.1. Adsorption System and Experimental Conditions

The illustrative case involved NH_4^+ adsorption onto corn-husk particles with sizes of 105, 250, and 500 µm. Initial concentrations (C_0) were 10, 20, 40, 60, and 80 mg/L, with a solution volume of 300 mL and an adsorbent mass of 3 g. Contact times ranged from 0 to 150 min. The conditions are summarized in **Table 8**.

The residual concentration generally decreased with increasing contact time, indicating progressive adsorbate removal (**Figure 7**). Smaller particles exhibited faster concentration decreases, consistent with shorter diffusion pathways and greater external surface area per unit adsorbent mass. However, particle-size dependence alone does not establish the controlling mass-transfer mechanism.

3.6.2. Adsorption Kinetics

Adsorption kinetics describes the variation in adsorption capacity with contact time. For a batch system with constant solution volume, the adsorption capacity (q_t) is calculated from the difference between the initial (C_0) and residual (C_t) concentrations: $q_t = \frac{(C_0 - C_t)V}{m}$. Differentiation with respect to time gives: $\frac{dq_t}{dt} = -\frac{V}{m}\frac{dC_t}{dt}$. Assuming that the remaining adsorption capacity (q_e-q_t) represents the kinetic driving term, a generalized empirical kinetic expression can be written as: $\frac{dq_t}{dt} = k_n(q_e - q_t)^n$, where q_e is the equilibrium adsorption capacity, k_n is the apparent kinetic constant, and n is the kinetic order.

Table 8. Conditions used in the illustrative adsorption case study (V = 300 mL; m = 3 g).

PARTICLE SIZE (µm)	*t* (min)	C_t (mg/L)	$q_t = \frac{(C_0 - C_t)V}{m}$ (mg/g)
105	0	10.00	0.000
	5	7.65	0.235
	10	5.87	0.413
	20	3.48	0.652
	30	2.10	0.790
	60	0.59	0.941
	90	0.30	0.970
	120	0.24	0.976
	150	0.22	0.978
250	0	10.00	0.000
	5	8.31	0.169
	10	6.91	0.309
	20	4.80	0.520
	30	3.35	0.665
	60	1.23	0.877
	90	0.55	0.945
	120	0.33	0.967
	150	0.30	0.970
500	0	10.00	0.000
	5	8.85	0.115
	10	7.84	0.216
	20	6.15	0.385
	30	4.84	0.516
	60	2.41	0.759
	90	1.26	0.874
	120	0.71	0.929
	150	0.66	0.934

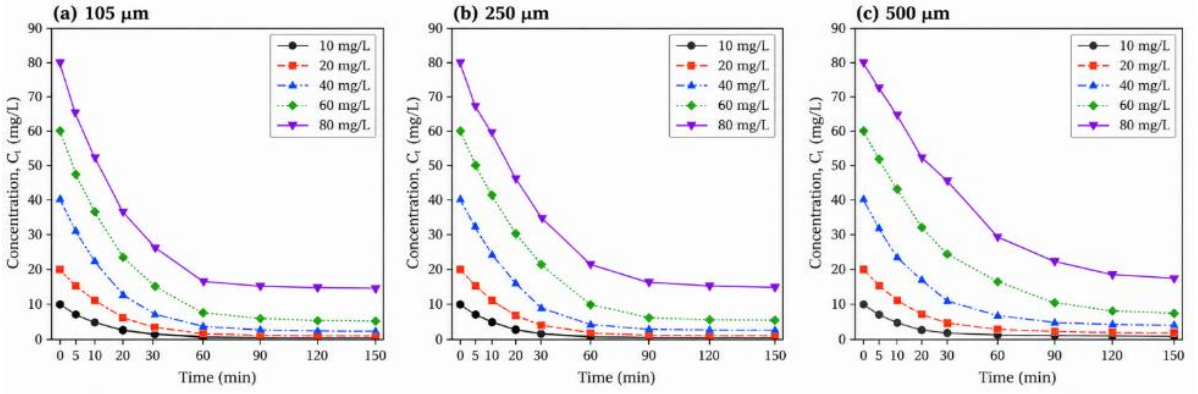


Figure 7. Concentration-time profiles for NH_4^+ adsorption onto corn-husk with particle sizes of (a) 105, (b) 250, and (c) 500 µm at initial concentrations of 10, 20, 40, 60, and 80 mg/L.

The pseudo-first-order (PFO), pseudo-second-order (PSO), and Elovich models were employed to examine adsorption behavior. Their principal equations and fitting parameters are shown in **Table 9**. The equilibrium adsorption capacity (q_e) must be assigned from the regression of the PFO, PSO, and Elovich models using the same adsorption-capacity data. The resulting fitted curves are compared in **Figure 8**, whereas the corresponding regression parameters and goodness-of-fit indicators are shown in **Table 10**. The best-fit values were approximately 0.9775, 0.9756, and 0.9656 mg/g for 105, 250, and 500 µm, respectively.

Table 9. Summary of kinetic equations and fitting parameters.

PARAMETER	PFO	PSO	ELOVICH
Differential equation	$\frac{dq_t}{dt} = k_1(q_e - q_t)$	$\frac{dq_t}{dt} = k_2(q_e - q_t)^2$	$\frac{dq_t}{dt} = \alpha e^{-\beta q_t}$
Linearized equation	$\ln(q_e - q_t) = \ln q_e - k_1 t$	$\frac{t}{q_t} = \frac{1}{k_2 q_e^2} + \frac{t}{q_e}$	$q_t = \frac{\ln(\alpha\beta)}{\beta} + \frac{\ln t}{\beta}$
X-axis	t	T	$\ln t$
Y-axis	$\ln(q_e\text{-}q_t)$	t/q_t	q_t
Slope	$-k_1$	$1/q_e$	$1/\beta$
Intercept	$\ln q_e$	$1/(k_2 q_e^2)$	$\ln(\alpha\beta)/\beta$
Nonlinear equation	$q_t = q_e(1 - e^{-k_1 t})$	$q_t = \frac{k_2 q_e^2 t}{1 + k_2 q_e t}$	$q_t = \frac{\ln(1 + \alpha\beta t)}{\beta}$
Rate constants	k_1 (1/min)	k_2 (g/mg.min)	α (mg/g.min), β (g/mg)

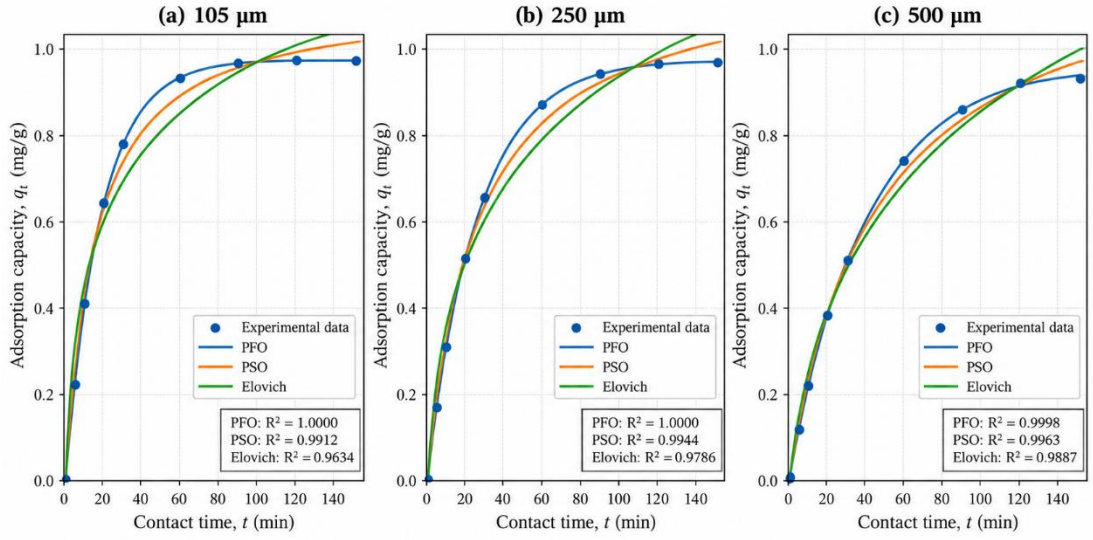


Figure 8. Nonlinear pseudo-first-order (PFO) fitting of NH_4^+ adsorption onto corn husk with sizes of (a) 105, (b) 250, and (c) 500 µm at C_0 of 10 mg/L. Data were taken from **Table 8**.

Table 10. Comparison of nonlinear kinetic-model fitting, regression equations, coefficients of determination, and equilibrium adsorption capacities for C_0 = 10 mg/L.

PARTICLE SIZE (µm)	KINETIC MODEL	FITTED REGRESSION EQUATION	R^2	$q_e = \lim_{t\to\infty} q_t$ (mg/g)
105	PFO	$q_t = 0.97748(1 - e^{-0.054972t})$	1.0000*	0.97748*
	PSO	$q_t = \frac{0.073954t}{1 + 0.065851t}$	0.9912	1.12317
	Elovich	$q_t = \frac{\ln(1 + 0.59353t)}{4.21426}$	0.9634	∞
250	PFO	$q_t = 0.97563(1 - e^{-0.038125t})$	1.0000*	0.97563*
	PSO	$q_t = \frac{0.047439t}{1 + 0.040254t}$	0.9944	1.17854
	Elovich	$q_t = \frac{\ln(1 + 0.24223t)}{3.44734}$	0.9786	∞
500	PFO	$q_t = 0.96562(1 - e^{-0.025604t})$	0.9998*	0.96562*
	PSO	$q_t = \frac{0.029219t}{1 + 0.023360t}$	0.9963	1.25079
	Elovich	$q_t = \frac{\ln(1 + 0.10244t)}{2.79627}$	0.9887	∞

Note: *the highest R^2 and the most fitted values

The transformed kinetic variables were subsequently calculated using the equations in **Table 9**. For this illustration, an initial concentration of 10 mg/L was selected, and the calculated values of q_t, ln(q_e-q_t), t/q_t, and ln t are presented in **Table 11**. The corresponding linear regression plots are shown in **Figure 9**. The PFO model exhibited strong correlations for all three sizes, with reported R^2 values ranging from approximately 0.987 to 1.000. However, the transformed-scale R^2 values from PFO, PSO, and Elovich regressions are not directly comparable because their dependent variables differ. Therefore, these results demonstrate the agreement of each linearized equation with its transformed data rather than conclusively identifying a superior kinetic model or adsorption mechanism.

Table 11. Calculation of adsorption kinetics (C_0 = 10 mg/L, V = 0.300 L, m = 3 g, and q_e = 0.9775, 0.9756, and 0.9656 mg/g for 105, 250, and 500 µm, respectively (from nonlinear fitting in **Table 10**)).

PARTICLE SIZE (µm)	t (min)	C_t (mg/L)	q_t (mg/g)	q_e-q_t (mg/g)	PFO: ln(q_e-q_t)	PSO: t/q_t	Elovich: ln t
105	0	10.00	0.000	0.9775	−0.0228	—	—
	5	7.65	0.235	0.7425	−0.2977	21.277	1.6094
	10	5.87	0.413	0.5645	−0.5718	24.213	2.3026
	20	3.48	0.652	0.3255	−1.1224	30.675	2.9957
	30	2.10	0.790	0.1875	−1.6740	37.975	3.4012
	60	0.59	0.941	0.0365	−3.3104	63.762	4.0943
	90	0.30	0.970	0.0075	−4.8929	92.784	4.4998
	120	0.24	0.976	0.0015	−6.5023	122.951	4.7875
	150	0.22	0.978	−0.0005	—	153.374	5.0106
250	0	10.00	0.000	0.9756	−0.0247	—	—
	5	8.31	0.169	0.8066	−0.2149	29.586	1.6094
	10	6.91	0.309	0.6666	−0.4056	32.362	2.3026
	20	4.80	0.520	0.4556	−0.7861	38.462	2.9957
	30	3.35	0.665	0.3106	−1.1692	45.113	3.4012
	60	1.23	0.877	0.0986	−2.3167	68.415	4.0943
	90	0.55	0.945	0.0306	−3.4868	95.238	4.4998
	120	0.33	0.967	0.0086	−4.7560	124.095	4.7875
	150	0.30	0.970	0.0056	−5.1850	154.639	5.0106
500	0	10.00	0.000	0.9656	−0.0350	—	—
	5	8.85	0.115	0.8506	−0.1618	43.478	1.6094
	10	7.84	0.216	0.7496	−0.2882	46.296	2.3026
	20	6.15	0.385	0.5806	−0.5437	51.948	2.9957
	30	4.84	0.516	0.4496	−0.7994	58.140	3.4012
	60	2.41	0.759	0.2066	−1.5770	79.051	4.0943
	90	1.26	0.874	0.0916	−2.3903	102.975	4.4998
	120	0.71	0.929	0.0366	−3.3077	129.171	4.7875
	150	0.66	0.934	0.0316	−3.4546	160.600	5.0106

3.6.3. Weber-Morris Analysis

The Weber-Morris model was applied to evaluate intraparticle diffusion and identify possible mass-transfer stages during adsorption. The model relates adsorption capacity (q_t) to the square root of contact time ($t^{½}$), as expressed $q_t = k_{id}t^{1/2} + I$, where k_{id} is the apparent intraparticle-diffusion rate constant (mg/g.min^{½}), and I is the intercept (mg/g). A larger k_{id} indicates faster apparent uptake within the corresponding region, whereas a nonzero intercept indicates that intraparticle diffusion may not be the only transport contribution.

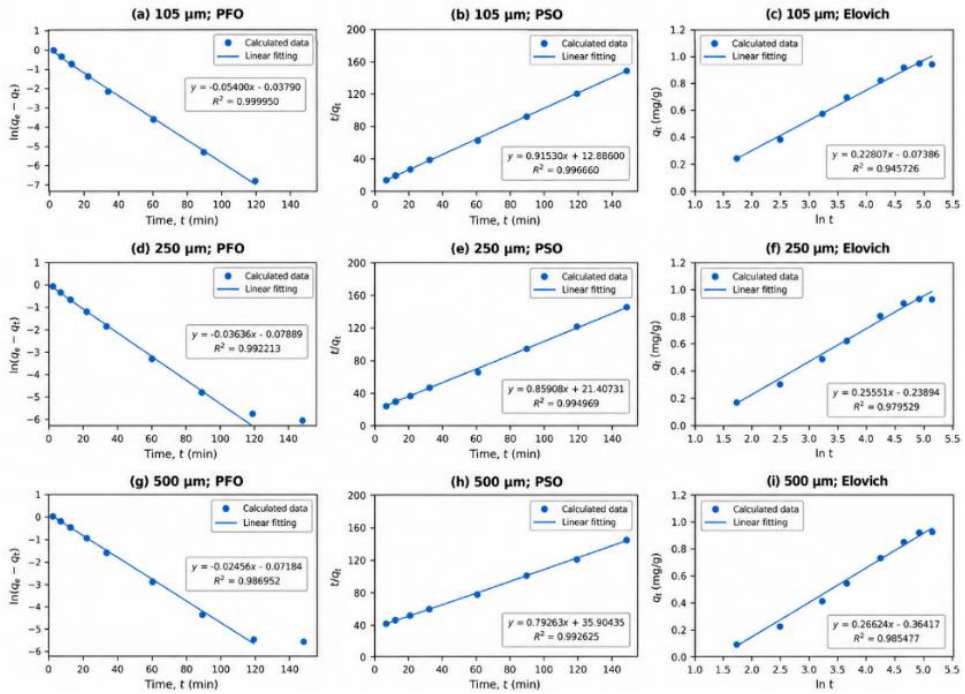


Figure 9. Linear regression plots of PFO, PSO, and Elovich adsorption kinetics at C_0 of 10 mg/L for particle sizes of 105 µm (a-c), 250 µm (d-f), and 500 µm (g-i), respectively.

Table 11. Calculation of Weber-Morris variables for different particle sizes at C_0 of 10 mg/L.

PARTICLE SIZE (µm)	*t* (min)	C_t (mg/L)	C_o–C_t (mg/L)	q_t (mg/g)	$t^{1/2}$ (min$^{1/2}$)
105	0	10.00	0.00	0.000	0.000
	5	7.65	2.35	0.235	2.236
	10	5.87	4.13	0.413	3.162
	20	3.48	6.52	0.652	4.472
	30	2.10	7.90	0.790	5.477
	60	0.59	9.41	0.941	7.746
	90	0.30	9.70	0.970	9.487
	120	0.24	9.76	0.976	10.954
	150	0.22	9.78	0.978	12.247
250	0	10.00	0.00	0.000	0.000
	5	8.31	1.69	0.169	2.236
	10	6.91	3.09	0.309	3.162
	20	4.80	5.20	0.520	4.472
	30	3.35	6.65	0.665	5.477
	60	1.23	8.77	0.877	7.746
	90	0.55	9.45	0.945	9.487
	120	0.33	9.67	0.967	10.954
	150	0.30	9.70	0.970	12.247
500	0	10.00	0.00	0.000	0.000
	5	8.85	1.15	0.115	2.236
	10	7.84	2.16	0.216	3.162
	20	6.15	3.85	0.385	4.472
	30	4.84	5.16	0.516	5.477
	60	2.41	7.59	0.759	7.746
	90	1.26	8.74	0.874	9.487
	120	0.71	9.29	0.929	10.954
	150	0.66	9.34	0.934	12.247

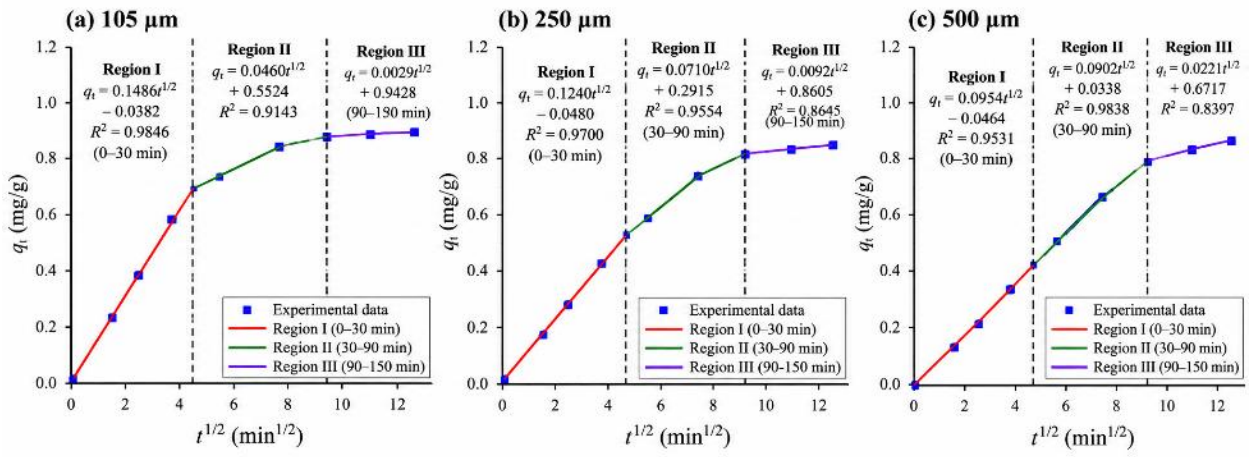


Figure 10. Weber-Morris plots of q_t vs $t^{½}$ for particle sizes of (a) 105, (b) 250, and (c) 500 µm.

The adsorption capacities and square-root contact times calculated from the concentration data are summarized in **Table 12**. The relationship between q_t and $t^{½}$ is shown in **Figure 10**. The profiles were divided into several regions, corresponding to rapid initial uptake, intermediate adsorption, and the final approach toward equilibrium. These intervals were based on the calculation (linear regression) to determine k_{id}, I, and the coefficient of determination R^2.

The resulting parameters are summarized in **Table 13**, providing findings:

(i) Region I exhibited relatively high k_{id} values, decreasing from 0.1486 to 0.0954 mg/g.min^{½} as particle size increased from 105 to 500 µm, indicating faster initial uptake for smaller particles;

(ii) Region II showed continued adsorption with reduced slopes, consistent with slower uptake and possible intraparticle-transport contributions; and

(iii) Region III exhibited the lowest slopes, indicating that adsorption approached equilibrium.

The nonzero intercepts and changes in slope suggest multiple transport contributions rather than a single diffusion process. However, the Weber-Morris model alone cannot conclusively identify the dominant rate-controlling mechanism

Table 13. Three-region Weber-Morris regression parameters at C_0 of 10 mg/L.

PARTICLE SIZE (µm)	REGION	TIME RANGE (min)	$t^{1/2}$ RANGE (min$^{1/2}$)	k_{id} (mg/g. min$^{1/2}$)	INTERCEPT I (mg/g)	R^2
105	I	0-30	0.00-5.48	0.1486	−0.0382	0.9846
	II	30-90	5.48-9.49	0.0460	0.5524	0.9143
	III	90-150	9.49-12.25	0.0029	0.9428	0.9414
250	I	0-30	0.00-5.48	0.1240	−0.0480	0.9700
	II	30-90	5.48-9.49	0.0710	0.2915	0.9554
	III	90-150	9.49-12.25	0.0092	0.8605	0.8645
500	I	0-30	0.00-5.48	0.0954	−0.0464	0.9531
	II	30-90	5.48-9.49	0.0902	0.0338	0.9838
	III	90-150	9.49-12.25	0.0221	0.6717	0.8397

3.6.4. Boyd Model Analysis

The Boyd model was applied to evaluate whether adsorption was predominantly controlled by intraparticle diffusion or influenced by external-film resistance. The fractional adsorption (F) was calculated from q_t/q_e, where q_e was obtained from the nonlinear PFO fitting. The Boyd function (B_t) was calculated using the following equations:

(i) For $F \leq 0.85$: $B_t = \left[\sqrt{\pi} - \sqrt{\pi - \frac{\pi^2 F}{3}}\right]^2$

(ii) For $0.85 < F < 1$\): $B_t = -0.4977 - \ln(1 - F)$

The calculated fractional adsorption and Boyd parameters are summarized in **Table 14**. The resulting B_t values were plotted against contact time using the linear equation $B_t = a.t + b$, where a is the slope and b is the intercept (**Figure 11**).

Table 14. Boyd transformation of adsorption data at an initial concentration of 10 mg/L using nonlinear-fitted equilibrium adsorption capacities.

PARTICLE SIZE (µm)	t (min)	q_t (mg/g)	$F = q_t/q_e$	B_t
105	0	0.000	0.000	0.000
	5	0.235	0.240	0.057
	10	0.413	0.423	0.202
	20	0.652	0.667	0.639
	30	0.790	0.808	1.161
	60	0.941	0.963	2.791
	90	0.970	0.992	4.375
	120	0.976	0.998	5.996
	150	0.978	1.001	—
250	0	0.000	0.000	0.000
	5	0.169	0.173	0.028
	10	0.309	0.317	0.105
	20	0.520	0.533	0.353
	30	0.665	0.682	0.679
	60	0.877	0.899	1.794
	90	0.945	0.969	2.963
	120	0.967	0.991	4.230
	150	0.970	0.994	4.657
500	0	0.000	0.000	0.000
	5	0.115	0.119	0.013
	10	0.216	0.224	0.049
	20	0.385	0.399	0.176
	30	0.516	0.534	0.355
	60	0.759	0.786	1.055
	90	0.874	0.905	1.857
	120	0.929	0.962	2.774
	150	0.934	0.967	2.921

Note: q_e were 0.9774788, 0.9756299, and 0.9656206 mg/g for 105, 250, and 500 µm, respectively (from fitting analysis explained above).

The fractional adsorption profiles, Boyd plots, early-stage adsorption behavior, and corresponding regression parameters are presented in **Figures 11(a-d)**. A regression line passing approximately through the origin is consistent with predominant intraparticle-diffusion control under the Boyd model assumptions, whereas a nonzero intercept suggests

additional transport resistance. The fractional adsorption increased with contact time for all particle sizes, with smaller particles approaching the fitted equilibrium capacity more rapidly. The results indicate several points:

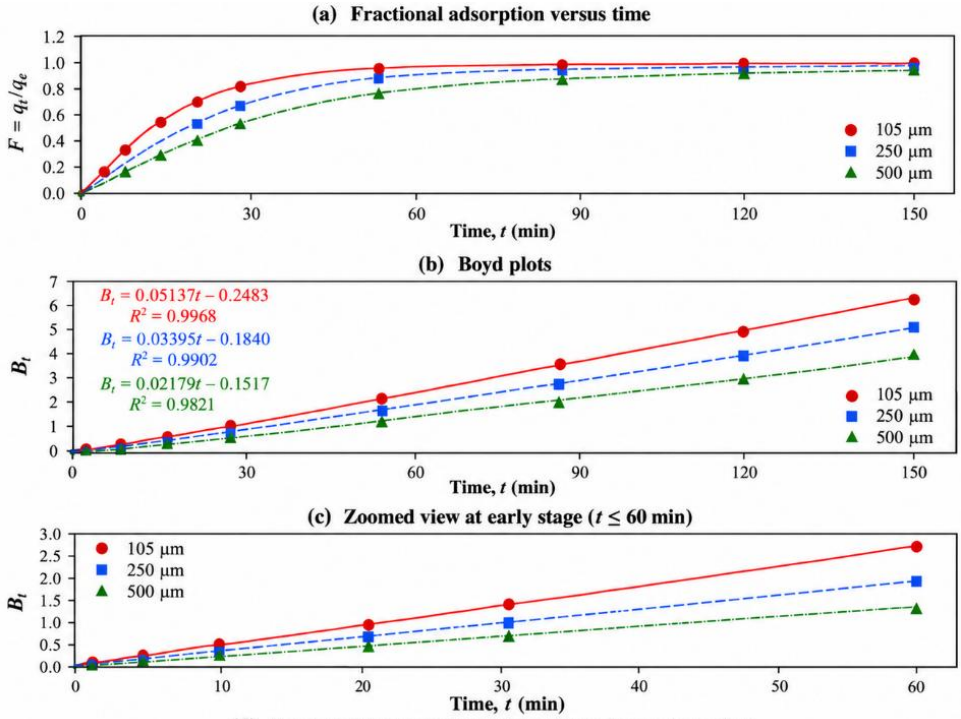
(i) the Boyd slope decreased from 0.05137 to 0.02179 1/min as size increased from 105 to 500 µm, indicating slower apparent transport progression for larger particles;

(ii) all regression lines exhibited negative intercepts, suggesting that intraparticle diffusion was not the only contributing resistance; and

(iii) the relatively high R^2 values indicate good linear agreement within the selected fitting ranges. However, the intercepts alone cannot quantify external-film resistance or establish a unique rate-controlling mechanism.

3.6.5. Fulazzaky Mass-Transfer Analysis

The Generalized Fulazzaky model was applied to evaluate the time-dependent mass-transfer behavior during adsorption. Following the Weber-Morris and Boyd analyses, this approach provides additional information on apparent external-film, global, and internal-derived mass-transfer factors. The model uses the logarithmic relationship between adsorption capacity (q_t) and contact time (t), expressed as $\ln(q_t) = B + \frac{1}{\beta}\ln(t)$, where B is the regression intercept and β is calculated from the reciprocal of the slope. Since ln(0) is undefined, data at t = 0 were excluded.



(d) Boyd model parameters obtained from linear regression

Particle size (µm)	Boyd equation	Slope (min^{-1})	Intercept	R^2
105	$B_t = 0.05137t - 0.2483$	0.05137	−0.2483	0.9968
250	$B_t = 0.03395t - 0.1840$	0.03395	−0.1840	0.9902
500	$B_t = 0.02179t - 0.1517$	0.02179	−0.1517	0.9821

Figure 11. Boyd analysis of adsorption at C_0 of 10 mg/L for sizes of 105, 250, and 500 µm: (a) fractional adsorption ($F = q_t/q_e$) versus t; (b) Boyd plots (B_t) vs t with linear regression; (c) enlarged view of the early adsorption stage (t < 60 min); and (d) summary of Boyd regression.

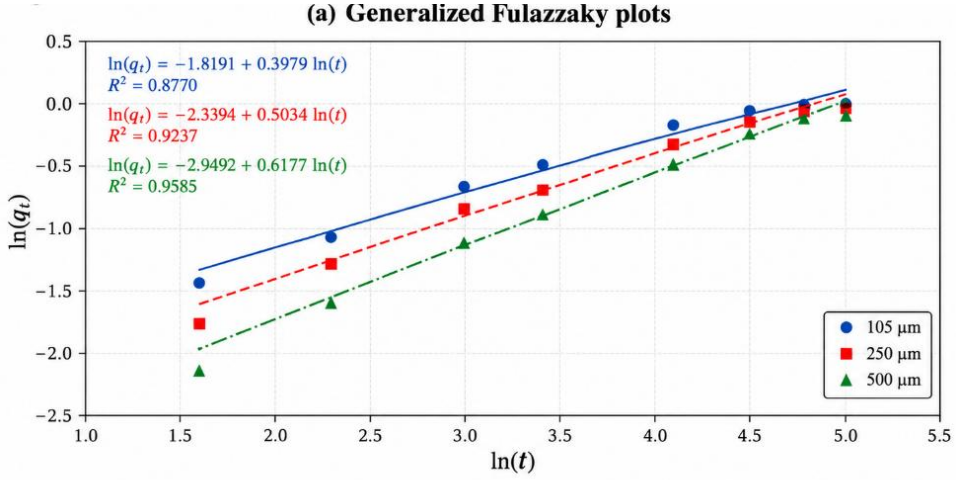
The combined regression plots for different particle sizes and their corresponding parameters are presented in **Figures 12(a) and (b)**. β decreased from 2.5134 to 1.6188 as particle size increased from 105 to 500 µm, while R^2 increased from 0.8770 to 0.9585. The logarithmic relationship describes the adsorption behavior with different degrees of agreement depending on particle size. The calculated β values were subsequently used to determine three mass-transfer factors (see **Figure 13**):

(i) External-film mass-transfer factor: $[k_L a]_f = \frac{\ln(C_0/C_t)}{t}$.

(ii) Global mass-transfer factor: $[k_L a]_g = [k_L a]_f q_t^{\beta}$.

(iii) Internal-derived mass-transfer: $[k_L a]_d = [k_L a]_g - [k_L a]_f$.

(a) Generalized Fulazzaky plots



(b) Regression parameters obtained from linear regression

Particle size (µm)	Regression equation	*B*	1/*β*	*β*	R^2
105	$\ln(q_t) = -1.8191 + 0.3979 \ln(t)$	-1.8191	0.3979	2.5134	0.8770
250	$\ln(q_t) = -2.3394 + 0.5034 \ln(t)$	-2.3394	0.5034	1.9864	0.9237
500	$\ln(q_t) = -2.9492 + 0.6177 \ln(t)$	-2.9492	0.6177	1.6188	0.9585

Figure 12. Fulazzaky analysis of adsorption onto corn-husk particles at C_0 of 10 mg/L: (a) combined plots of ln(q_t) versus ln t for particle sizes of 105, 250, and 500 µm, including their linear regression lines; and (b) corresponding regression equations, intercepts (B), slopes ($1/\beta$), β values, and coefficients of determination (R^2).

The calculated mass-transfer factors are summarized in **Table 15**. These relationships are schematically illustrated in **Figure 14**. The results indicate three main findings:

(i) $[k_L a]_f$ generally decreased with increasing particle size, indicating slower apparent concentration depletion for larger particles;

(ii) $[k_L a]_g$ increased during the initial adsorption period before decreasing at longer contact times; and

(iii) $[k_L a]_d$ remained negative but approached zero as adsorption progressed, indicating convergence between the calculated global and external-film factors. A negative $[k_L a]_d$ does not represent negative diffusion or desorption.

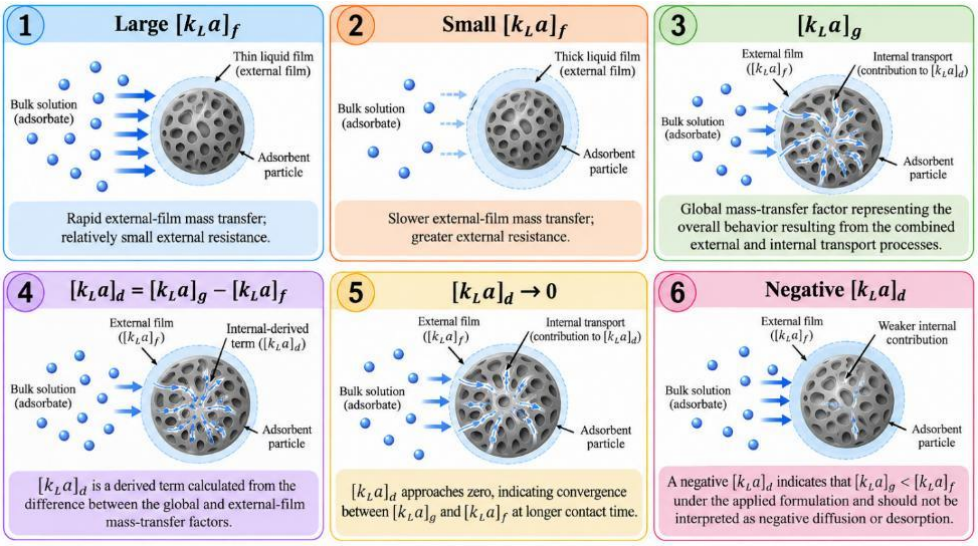


Figure 13. Schematic interpretation of the mass-transfer factors obtained from the Fulazzaky analysis: (1) relatively large $[k_La]_f$, indicating rapid external-film transport and relatively small external resistance; (2) relatively small $[k_La]_f$, indicating slower external-film transport and greater external resistance; (3) $[k_La]_g$, representing the global mass-transfer behavior; (4) $[k_La]_d = [k_La]_g - [k_La]_f$, representing the internal-derived mass-transfer term; (5) $[k_La]_f$ near to 0, indicating convergence between $[k_La]_g$ and $[k_La]_f$; and (6) negative $[k_La]_d$, indicating $[k_La]_g < [k_La]_f$ rather than negative diffusion.

Table 15. External-film, global, and internal-derived mass-transfer factors calculated for NH_4^+ adsorption at an initial concentration of 10 mg/L.

PARTICLE SIZE (μm)	t (min)	C_t (mg/L)	q_t (mg/g)	$[k_La]_f$ (1/min)	$[k_La]_g$ (1/min)	$[k_La]_d$ (1/min)
105	5	7.65	0.235	0.0536	0.0014	−0.0522
	10	5.87	0.413	0.0533	0.0058	−0.0475
	20	3.48	0.652	0.0528	0.0180	−0.0348
	30	2.10	0.790	0.0520	0.0288	−0.0233
	60	0.59	0.941	0.0472	0.0405	−0.0067
	90	0.30	0.970	0.0390	0.0361	−0.0029
	120	0.24	0.976	0.0311	0.0292	−0.0018
	150	0.22	0.978	0.0254	0.0241	−0.0014
250	5	8.31	0.169	0.0370	0.0011	−0.0359
	10	6.91	0.309	0.0370	0.0036	−0.0334
	20	4.80	0.520	0.0367	0.0100	−0.0267
	30	3.35	0.665	0.0365	0.0162	−0.0202
	60	1.23	0.877	0.0349	0.0269	−0.0080
	90	0.55	0.945	0.0322	0.0288	−0.0034
	120	0.33	0.967	0.0284	0.0266	−0.0018
	150	0.30	0.970	0.0234	0.0220	−0.0014
500	5	8.85	0.115	0.0244	0.0007	−0.0237
	10	7.84	0.216	0.0243	0.0020	−0.0223
	20	6.15	0.385	0.0243	0.0052	−0.0191
	30	4.84	0.516	0.0242	0.0083	−0.0159
	60	2.41	0.759	0.0237	0.0152	−0.0085
	90	1.26	0.874	0.0230	0.0185	−0.0045
	120	0.71	0.929	0.0220	0.0196	−0.0025
	150	0.66	0.934	0.0181	0.0162	−0.0019

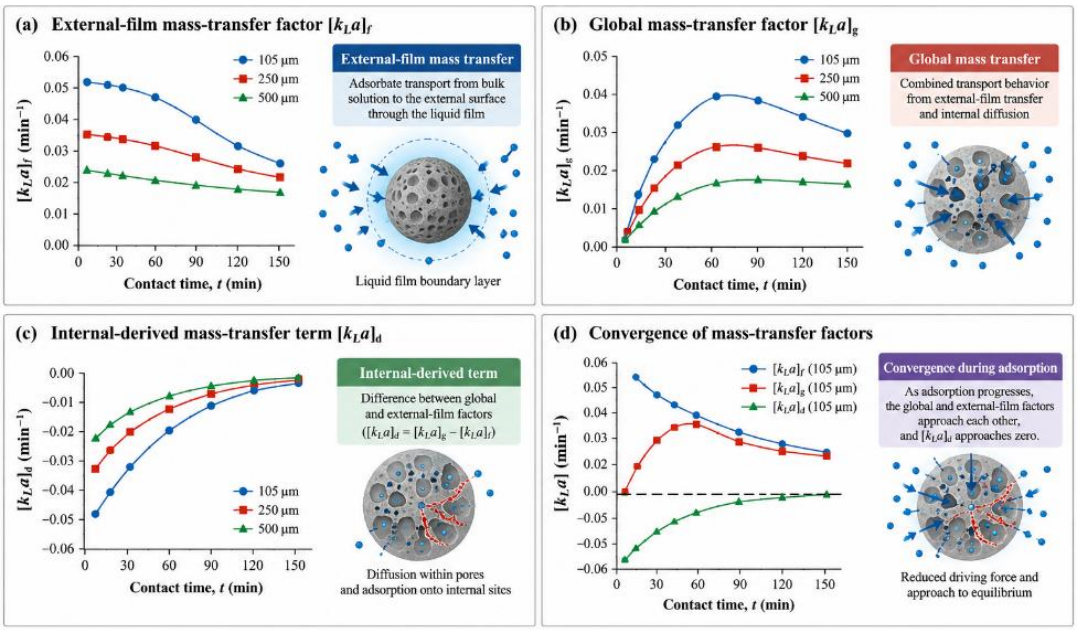


Figure 14. Fulazzaky mass-transfer analysis for NH_4^+ adsorption onto corn-husk particles: (a) external-film mass-transfer factor $[k_La]_f$, (b) global mass-transfer factor $[k_La]_g$, (c) internal-derived mass-transfer term $[k_La]_d$, and (d) convergence of the calculated mass-transfer factors during adsorption. The plots compare particle sizes of 105, 250, and 500 µm at C_0 of 10 mg/L, accompanied by schematic illustrations of the corresponding transport processes.

3.6.6. Nandiyanto Mass-Transfer Classification

Unlike the Fulazzaky approach, the Nandiyanto mass-transfer classification employs normalized concentration and adsorption-capacity parameters to provide a more general framework for comparing adsorption systems with different adsorption capacities. Normalization reduces the dependence of the calculated mass-transfer factors on the absolute adsorption capacity. The analysis begins with the calculation of normalized concentration and adsorption capacity, followed by the determination of normalized mass-transfer factors and the adsorption-progress index. The basic calculation results are summarized in **Table 16**, while the regression analysis used to determine the normalized exponent (β*) is presented in **Figure 15**.

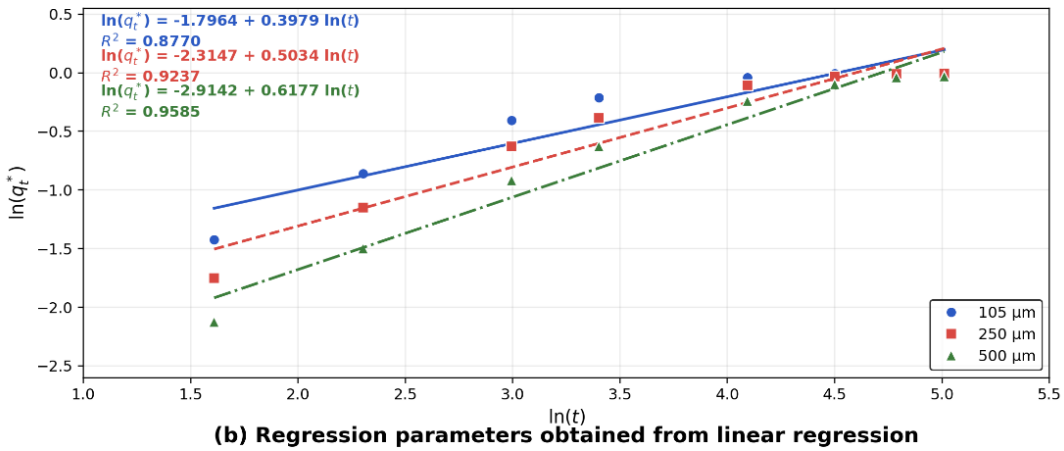
The normalized residual concentration (C_t*) and normalized adsorption capacity (q_t*) are defined as $C_t^* = \frac{C_t - C_e}{C_0 - C_e}$ and $q_t^* = \frac{q_t}{q_e} = \frac{C_0 - C_t}{C_0 - C_e} = 1 - C_t^*$, where C_o, C_t, and C_e are the initial, time-dependent, and equilibrium adsorbate concentrations, respectively, while q_t and q_e represent the adsorption capacities at time t and at equilibrium. Both normalized parameters are dimensionless. Under the assumed batch mass balance, C_t* decreases from unity toward zero, whereas q_t* increases from zero toward unity as adsorption approaches equilibrium.

The normalized exponent (β*) is obtained from the linear regression of ln q_t* against ln t, expressed as: $\ln(q_t^*) = B^* + \frac{1}{\beta^*}\ln(t)$, where B* is the regression intercept and 1/β* is the regression slope. The calculated β* values are 2.5134, 1.9864, and 1.6188 for particle sizes of 105, 250, and 500 µm, respectively, as shown in **Figure 15**.

Table 16. Calculation of normalized concentration, adsorption capacity, and Nandiyanto mass-transfer factors for NH_4^+ adsorption onto corn-husk particles (C_o = 10 mg/L (V = 0.300 L and m = 3 g). The fitted q_e values are 0.9774788, 0.9756299, and 0.9656206 mg/g, while β values (see **Figure 15**) are 2.5134, 1.9864, and 1.6188 for particle sizes of 105, 250, and 500 µm, respectively.

PARTICLE SIZE (µm)	t (min)	C_t (mg/L)	$q_t = (C_o - C_t)V/m$ (mg/g)	$C_t^* = (C_t - C_e)/(C_o - C_e)$	$q_t^* = q_t/q_e$	$[k_La]_f^* = -\ln(C_t^*)/t$ (1/min)	$[k_La]_g^* = [k_La]_f^*(q_t^*)^{\beta^*}$ (1/min)	$[k_La]_d^* = [k_La]_g^* - [k_La]_f^*$ (1/min)	$\Phi N^* = [k_La]_g^*/[k_La]_f^*$	Region
105	0	10.00	0.000	1.0000	0.0000	—	—	—	0.0000	I – Early
	5	7.65	0.235	0.7596	0.2404	0.0550	0.0015	−0.0535	0.0278	I – Early
	10	5.87	0.413	0.5775	0.4225	0.0549	0.0063	−0.0486	0.1147	I – Early
	20	3.48	0.652	0.3330	0.6670	0.0550	0.0199	−0.0351	0.3614	I – Early
	30	2.10	0.790	0.1918	0.8082	0.0550	0.0322	−0.0228	0.5855	II – Intermediate
	60	0.59	0.941	0.0373	0.9627	0.0548	0.0498	−0.0050	0.9088	III – Near-equilibrium
	90	0.30	0.970	0.0077	0.9923	0.0541	0.0531	−0.0010	0.9809	III – Near-equilibrium
	120	0.24	0.976	0.0015	0.9985	0.0541	0.0539	−0.0002	0.9962	III – Near-equilibrium
	150	0.22	0.978	−0.0005	1.0005	—	—	—	1.0013	III – Near-equilibrium
250	0	10.00	0.000	1.0000	0.0000	—	—	—	0.0000	I – Early
	5	8.31	0.169	0.8268	0.1732	0.0380	0.0012	−0.0369	0.0307	I – Early
	10	6.91	0.309	0.6833	0.3167	0.0381	0.0039	−0.0342	0.1019	I – Early
	20	4.80	0.520	0.4670	0.5330	0.0381	0.0109	−0.0272	0.2865	I – Early
	30	3.35	0.665	0.3184	0.6816	0.0381	0.0178	−0.0203	0.4670	I – Early
	60	1.23	0.877	0.1011	0.8989	0.0382	0.0309	−0.0073	0.8092	II – Intermediate
	90	0.55	0.945	0.0314	0.9686	0.0385	0.0361	−0.0024	0.9386	III – Near-equilibrium
	120	0.33	0.967	0.0088	0.9912	0.0394	0.0387	−0.0007	0.9825	III – Near-equilibrium
	150	0.30	0.970	0.0058	0.9942	0.0344	0.0340	−0.0004	0.9886	III – Near-equilibrium
500	0	10.00	0.000	1.0000	0.0000	—	—	—	0.0000	I – Early
	5	8.85	0.115	0.8809	0.1191	0.0254	0.0008	−0.0246	0.0319	I – Early
	10	7.84	0.216	0.7763	0.2237	0.0253	0.0022	−0.0231	0.0886	I – Early
	20	6.15	0.385	0.6013	0.3987	0.0254	0.0057	−0.0197	0.2257	I – Early
	30	4.84	0.516	0.4656	0.5344	0.0255	0.0092	−0.0162	0.3626	I – Early
	60	2.41	0.759	0.2140	0.7860	0.0257	0.0174	−0.0083	0.6772	II – Intermediate
	90	1.26	0.874	0.0949	0.9051	0.0262	0.0223	−0.0039	0.8510	II – Intermediate
	120	0.71	0.929	0.0379	0.9621	0.0273	0.0256	−0.0017	0.9393	III – Near-equilibrium
	150	0.66	0.934	0.0327	0.9673	0.0228	0.0216	−0.0012	0.9475	III – Near-equilibrium

(a) Linearization plots for determining β^*



(b) Regression parameters obtained from linear regression

Particle size (µm)	Regression equation	B^*	$1/\beta^*$	β^*	R^2
105	$\ln(q_t^*) = -1.7964 + 0.3979 \ln(t)$	-1.7964	0.3979	2.5134	0.8770
250	$\ln(q_t^*) = -2.3147 + 0.5034 \ln(t)$	-2.3147	0.5034	1.9864	0.9237
500	$\ln(q_t^*) = -2.9142 + 0.6177 \ln(t)$	-2.9142	0.6177	1.6188	0.9585

Figure 15. Normalized adsorption-capacity linearization for determining β*: (a) plots of ln(q_t*) vs ln(t) for particle sizes of 105, 250, and 500 µm, including linear regression lines; and (b) regression equations, intercepts (B*), slopes (1/β*), β* values, and coefficients of determination (R^2).

The normalized mass-transfer factors are subsequently calculated using the following equations:

(i) Normalized apparent external-film mass-transfer factor: $[k_L a]_f^* = \frac{-\ln(C_t^*)}{t}$

(ii) Normalized global mass-transfer factor: $[k_L a]_g^* = [k_L a]_f^* (q_t^*)^{\beta^*}$

(iii) Normalized internal-derived mass-transfer term: $[k_L a]_d^* = [k_L a]_g^* - [k_L a]_f^*$

These factors are expressed in min^{-1} when contact time is given in minutes. They are apparent, model-dependent parameters rather than independently measured external-film and internal-diffusion coefficients. The calculated profiles and their conceptual interpretations are presented in **Figure 16**.

The normalized Nandiyanto classification uses the ratio of the global and external-film factors to describe the relative progression of adsorption. The model provides the following parameters:

(i) Normalized mass-transfer progress index: $\Phi_N^* = \frac{[k_L a]_g^*}{[k_L a]_f^*} = (q_t^*)^{\beta^*}$. A low Φ_N* indicates that the calculated global mass-transfer factor is substantially lower than the apparent external-film factor. As Φ_N* approaches unity, the two factors converge. This convergence follows from the normalized mathematical formulation and provides an operational description of adsorption progression rather than independent evidence of a particular rate-controlling mechanism. Adsorption was classified into three operational stages:

- Region I (early stage): $\Phi_N^* < 0.50$.
- Region II (intermediate stage): $0.50 \leq \Phi_N^* < 0.90$.
- Region III (near-equilibrium stage): $\Phi_N^* \geq 0.90$.

(ii) Characteristic transition times: Φ_N (t_{50}) = 0.50 and Φ_N (t_{90}) = 0.90, where t_{50} represents the transition from the early to the intermediate stage, and t_{90} represents the

transition from the intermediate to the operational near-equilibrium stage. Both transition times were estimated by linear interpolation between the adjacent experimental data points surrounding the corresponding thresholds.

(iii) Intermediate-stage duration: $\Delta t_N = t_{90}\text{-}t_{50}$. The intermediate-stage duration represents the time required for the normalized progress index to increase from 0.50 to 0.90.

(iv) Transition rate: $R_N = \frac{0.90-0.50}{t_{90}-t_{50}} = \frac{0.40}{\Delta t_N}$. The transition rate ($R_N$) represents the average increase in the normalized progress index per unit time during the intermediate stage.

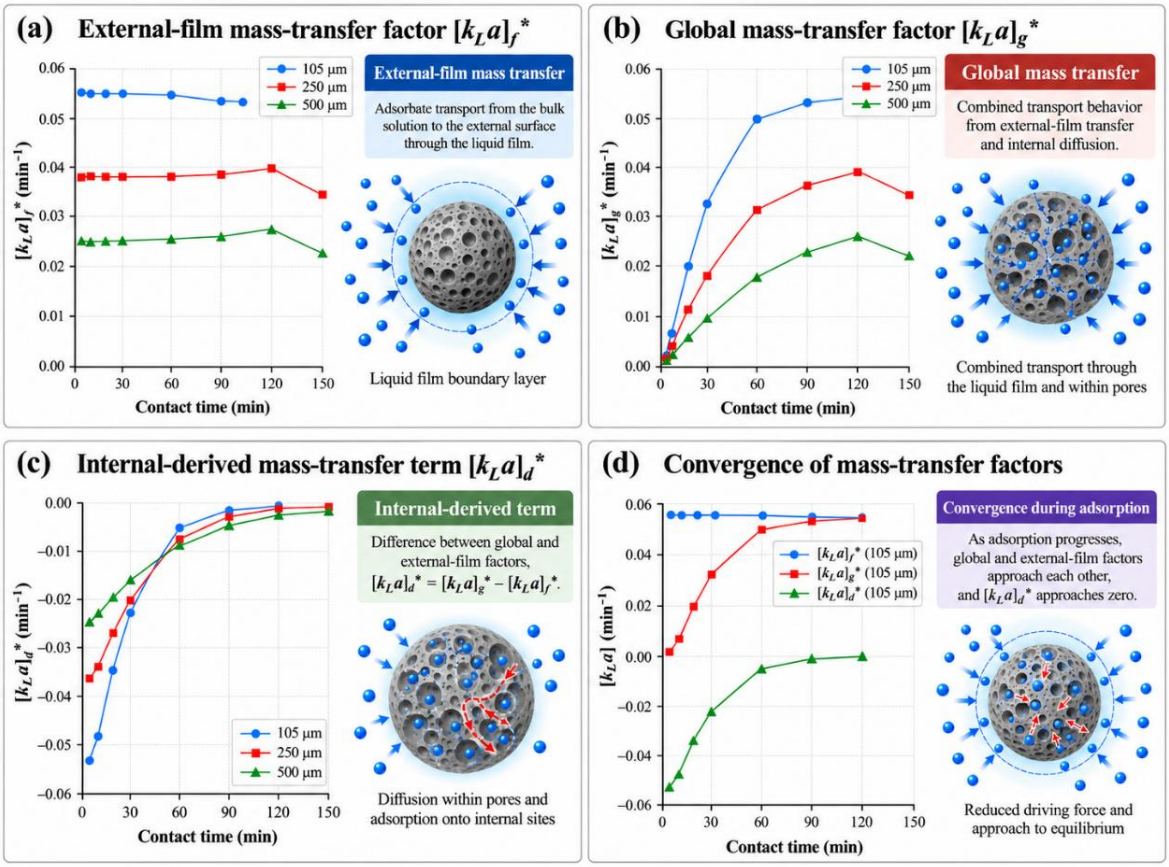


Figure 16. Normalized Nandiyanto mass-transfer analysis for adsorption onto corn-husk with sizes of 105, 250, and 500 µm: (a) normalized external-film mass-transfer factor ($[k_La]_f^*$); (b) normalized global mass-transfer factor ($[k_La]_g^*$); (c) normalized internal-derived mass-transfer term ($[k_La]_d^*$); and (d) convergence of normalized external-film, global, and internal-derived mass-transfer factors for 105-µm particles.

The calculated Φ_N^* values and corresponding adsorption regions are summarized in **Table 16**. The characteristic transition times (t_{50} and t_{90}), intermediate-stage duration (Δt_N), and transition rate (R_N) are presented in **Table 17**. The classification framework, transition parameters, normalized progress profiles, and schematic interpretations are illustrated in **Figure 17**. The characteristic transition times (t_{50} and t_{90}) increased with particle size, indicating slower relative adsorption progression for larger particles. The 105-µm particles exhibited the shortest transition duration, whereas the 500-µm particles required the longest time to reach the operational near-equilibrium stage. The usefulness of normalization for comparing adsorption progression across different particle sizes without directly relying on absolute adsorption capacity.

Table 17. Characteristic transition times, intermediate-stage duration, and transition rate obtained from the normalized Nandiyanto mass-transfer classification.

PARTICLE SIZE (μm)	t_{50} (min)	t_{90} (min)	Δt_N (min)	R_N (min^{-1})
105	26.18	59.18	33.00	0.01212
250	32.89	81.05	48.16	0.00831
500	43.10	106.65	63.55	0.00629

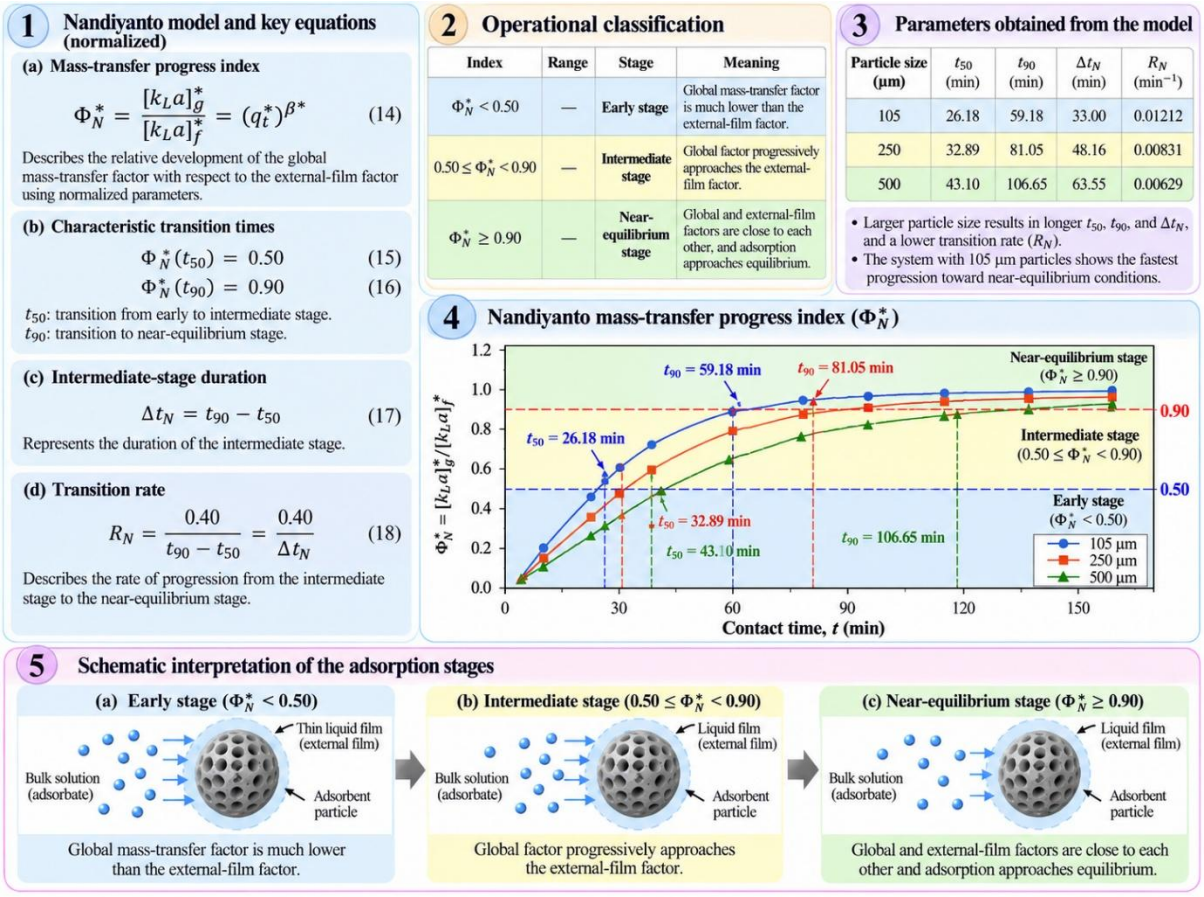


Figure 17. Normalized Nandiyanto mass-transfer classification for NH_4^+ adsorption onto corn-husk particles with sizes of 105, 250, and 500 μm: (1) normalized mass-transfer progress index and key equations; (2) operational classification into early, intermediate, and near-equilibrium adsorption stages; (3) calculated transition parameters, including t_{50}, t_{90}, intermediate-stage duration (Δt_N), and transition rate (R_N); (4) variation of the normalized mass-transfer progress index (Φ_N*) with contact time and identification of characteristic transition times; and (5) schematic interpretation of the three adsorption stages based on normalized mass-transfer progression.

The calculated transition parameters revealed a clear particle-size dependence. As particle size increased from 105 to 500 μm, t_{50} increased from 26.18 to 43.10 min, while t_{90} increased from 59.18 to 106.65 min. The intermediate-stage duration also increased from 33.00 to 63.55 min, accompanied by a decrease in the transition rate from 0.01212 to 0.00629 min^{-1}. Smaller particles exhibited faster normalized adsorption progression, whereas larger particles required longer contact times to approach the operational near-equilibrium stage. Although the normalized factors converged as adsorption progressed, this behavior should be interpreted as part of the proposed mathematical classification rather than direct confirmation of a specific mass-transfer mechanism.

3.6.7. Furusawa-Smith External Mass-Transfer Analysis

The Furusawa-Smith approach was applied to evaluate apparent external mass-transfer behavior during the initial adsorption stage. Two approaches were compared to determine the appropriate regression interval: (i) the first adsorption region identified by the Weber-Morris model and (ii) the early-stage boundary obtained from the Nandiyanto mass-transfer classification. This comparison was conducted to evaluate how the selection of adsorption intervals influences the calculated mass-transfer parameters. For a system described by a linear adsorption equilibrium relationship, the Furusawa-Smith model can be expressed as $\ln\left(\frac{C_t}{C_0}-\frac{1}{1+m_sK_L}\right)=\ln\left(\frac{m_sK_L}{1+m_sK_L}\right)-\frac{1+m_sK_L}{m_sK_L}k_fA_pt$, where m_s is the adsorbent mass per unit solution volume, K_L is the linear adsorption equilibrium constant, k_f is the external-film mass-transfer coefficient, and A_p represents the external interfacial area per unit solution volume. To simplify, k_fA_p can be written as k_{app}. For the practical example, a simplified concentration-decay expression was used to estimate an apparent external mass-transfer parameter: $\ln\left(\frac{C_t}{C_0}\right)=-k_fA_pt+b$ or $\ln\left(\frac{C_t}{C_0}\right)=-k_{app}t+b$. The apparent mass-transfer term (k_{app}), was obtained from the negative slope of the linear regression. The corresponding characteristic mass-transfer time was calculated using $\tau_f=\frac{1}{k_fA_p}$.

The two approaches differed in their criteria for selecting the initial adsorption interval (**Table 18**). The concentration data were transformed into ln(C_t/C_0) and linearly regressed against contact time. The resulting regression profiles and comparison of the two interval-selection approaches are illustrated in **Figure 18**. The regression parameters obtained using both approaches are summarized in **Table 19**. The results show several important findings.

(i) For the 105-µm particles, the two approaches produced slightly different apparent mass-transfer parameters because the normalized Nandiyanto approach selected a shorter regression interval (0–20 min), compared with the Weber-Morris interval (0–30 min). The calculated k_{app} increased from 0.05203 to 0.05274 min^{-1}, while the characteristic transfer time decreased from 19.22 to 18.96 min.

(ii) For the 250-µm particles, both approaches produced identical regression parameters because the same experimental time points (0, 5, 10, 20, and 30 min) were selected. The calculated k_{app} was 0.03645 min^{-1}, corresponding to a characteristic transfer time of 27.44 min.

(iii) For the 500-µm particles, both approaches used the same regression dataset and produced an apparent concentration-decay coefficient of 0.02419 min^{-1} and a characteristic transfer time of 41.33 min.

(iv) The influence of interval selection depended on particle size and the available sampling times. For the 105-µm particles, the normalized Nandiyanto approach selected fewer experimental data points than the Weber-Morris approach, resulting in slightly different regression parameters. For the 250- and 500-µm particles, both approaches selected identical regression datasets and therefore produced identical apparent concentration-decay coefficients. Interval selection and experimental sampling resolution influence the calculated apparent mass-transfer parameters.

Table 18. Comparison of initial adsorption intervals selected using Weber-Morris and Nandiyanto classifications.

PARTICLE SIZE (µm)	Weber-Morris Region I (min)	Nandiyanto t_{50} (min)	Weber-Morris regression data (min)	Nandiyanto regression data (min)
105	0-30	26.18	0, 5, 10, 20, 30	0, 5, 10, 20
250	0-30	32.89	0, 5, 10, 20, 30	0, 5, 10, 20, 30
500	0-30	43.10	0, 5, 10, 20, 30	0, 5, 10, 20, 30

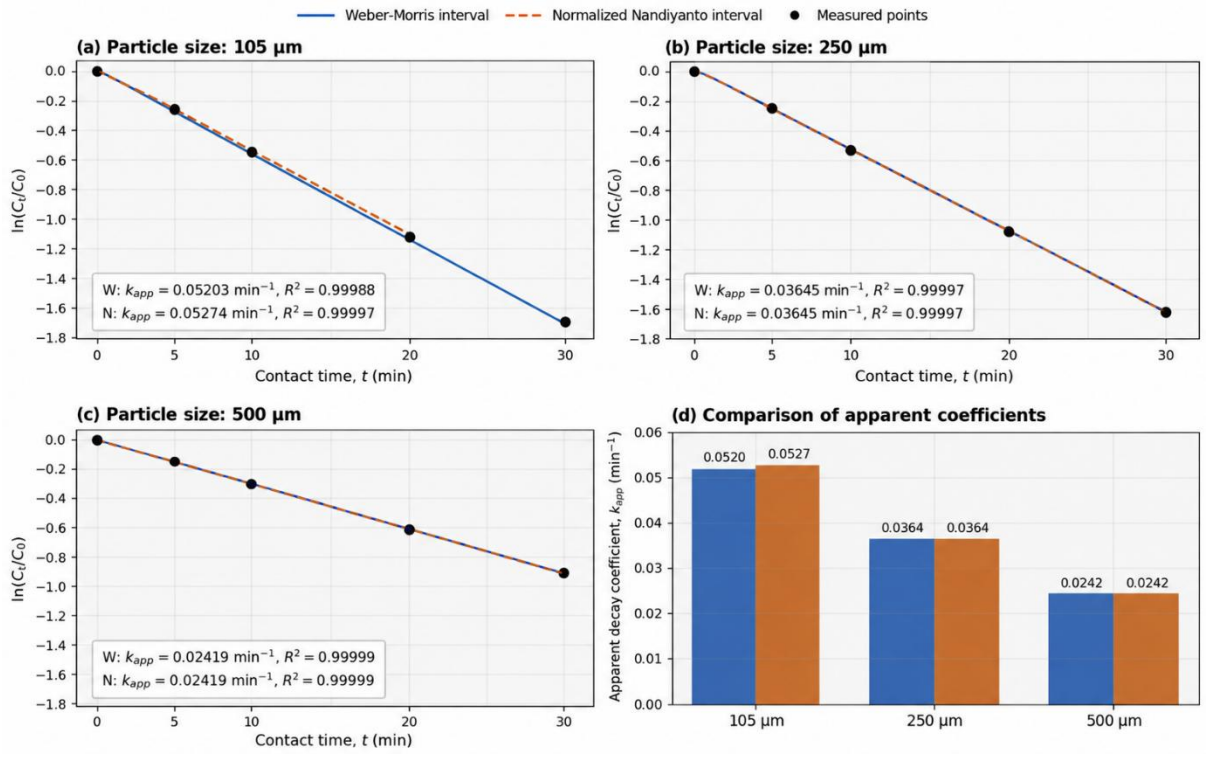


Figure 18. Comparison of apparent external mass-transfer analysis using Weber-Morris- and Nandiyanto-based regression intervals for NH_4^+ adsorption at C_0 of 10 mg/L onto corn-husk particles: (a) 105, (b) 250, and (c) 500 µm, and (d) comparison of the calculated apparent mass-transfer parameters and characteristic transfer times.

Table 19. Comparison of apparent external mass-transfer parameters obtained using Weber-Morris- and Nandiyanto-based regression intervals.

PARTICLE SIZE (µm)	APPROACH	REGRESSION EQUATION	R^2	k_{app} (1/min)	τ_f (min)
105	Weber-Morris	y = -0.05203t -0.00694	0.99988	0.05203	19.22
	Nandiyanto	y = -0.05274t -0.00259	0.99997	0.05274	18.96
250	Weber-Morris	y = -0.03645t - 0.00265	0.99997	0.03645	27.44
	Nandiyanto*	y = -0.03645t - 0.00265	0.99997	0.03645	27.44
500	Weber-Morris	y = -0.02419t - 0.00095	0.99999	0.02419	41.33
	Nandiyanto*	y = -0.02419t - 0.00095	0.99999	0.02419	41.33

3.6.8. Effective Diffusivity Analysis

Effective diffusivity (D_e) was evaluated to characterize the apparent internal transport of NH_4^+ within corn-husk particles. Unlike the Furusawa-Smith analysis, which focused on initial concentration depletion, the effective diffusivity analysis examined adsorption uptake in relation to particle size and the selected diffusion interval:

(i) overall effective diffusivity ($D_{e,O}$), calculated from the adsorption profile;

(ii) Weber-Morris-based effective diffusivity ($D_{e,W}$), evaluated within Region II; and

(iii) Nandiyanto-based effective diffusivity ($D_{e,N}$), evaluated within the operational intermediate adsorption stage.

These parameters were compared to determine how the selection of the regression interval influences the estimated internal transport characteristics. Assuming diffusion within approximately spherical particles, the fractional adsorption uptake can be expressed as $F = \frac{q_t}{q_e} = 1 - \frac{6}{\pi^2}\sum_{n=1}^{\infty}\frac{1}{n^2}\exp\left(-\frac{n^2\pi^2 D_e t}{R_p^2}\right)$, where F is fractional adsorption uptake, q_t is adsorption capacity at contact time t, q_e is equilibrium adsorption capacity, D_e is effective diffusivity, and R_p is particle radius. Using the first-term approximation, the equation becomes $\ln(1-F) = \ln\left(\frac{6}{\pi^2}\right) - \frac{\pi^2 D_e}{R_p^2}t$. The effective diffusivity was subsequently obtained from the slope of the linear regression $D_e = \frac{|s|R_p^2}{\pi^2}$, where s is the regression slope in 1/s. To facilitate interpretation, the characteristic diffusion time (τ_d) was calculated as $\tau_d = \frac{R_p^2}{D_e}$. A smaller τ_d represents a shorter characteristic diffusion timescale, whereas a larger value indicates a longer timescale for apparent internal transport. The transformed adsorption data used for the effective diffusivity analysis are summarized in **Table 20**. To compare the three approaches, separate linear regressions of ln(1-F) against contact time were performed for the overall adsorption interval, Weber-Morris Region II, and the Nandiyanto intermediate stage. The regression profiles are illustrated in **Figure 19**. The calculated effective diffusivity and characteristic diffusion time parameters are summarized in **Table 21**. The comparison of effective diffusivity and characteristic diffusion time is presented in **Figure 20**. The results can be summarized:

(i) The characteristic diffusion time τ_d indicates the apparent internal diffusion timescale. A smaller τ_d represents faster characteristic diffusion, whereas a larger value indicates slower diffusion.

(ii) Increasing particle size from 105 to 500 µm increased the characteristic diffusion time (τ_d) from 182.4 to 401.9 min for the overall approach, from 183.8 to 372.3 min for the Weber–Morris approach, and from 180.5 to 355.2 min for the normalized Nandiyanto approach. These results indicate longer characteristic diffusion timescales for larger particles across all three approaches.

(iii) The three diffusivity parameters differ in their regression intervals: $D_{e,O}$ represents overall adsorption, $D_{e,W}$ represents Weber-Morris Region II, and $D_{e,N}$ represents the Nandiyanto intermediate stage.

Although D_e increased with particle size, this does not necessarily indicate faster adsorption because D_e depends on the squared particle radius. Therefore, τ_d provides a more practical comparison of characteristic transport timescales.

Table 20. Fractional adsorption uptake and logarithmic variables for effective diffusivity.

PARTICLE SIZE (μm)	t (min)	q_t (mg/g)	q_e (mg/g)	$F = q_t/q_e$	$1 - F$	ln(1-F)
105	0	0.000	0.9775	0.000	1.000	0.000
	5	0.235	0.9775	0.240	0.760	−0.275
	10	0.413	0.9775	0.423	0.577	−0.549
	20	0.652	0.9775	0.667	0.333	−1.100
	30	0.790	0.9775	0.808	0.192	−1.651
	60	0.941	0.9775	0.963	0.037	−3.288
	90	0.970	0.9775	0.992	0.008	−4.870
	120	0.976	0.9775	0.998	0.002	−6.480
	150	0.978	0.9775	1.001	—	—
250	0	0.000	0.9756	0.000	1.000	0.000
	5	0.169	0.9756	0.173	0.827	−0.190
	10	0.309	0.9756	0.317	0.683	−0.381
	20	0.520	0.9756	0.533	0.467	−0.761
	30	0.665	0.9756	0.682	0.318	−1.145
	60	0.877	0.9756	0.899	0.101	−2.292
	90	0.945	0.9756	0.969	0.031	−3.462
	120	0.967	0.9756	0.991	0.009	−4.731
	150	0.970	0.9756	0.994	0.006	−5.160
500	0	0.000	0.9656	0.000	1.000	0.000
	5	0.115	0.9656	0.119	0.881	−0.127
	10	0.216	0.9656	0.224	0.776	−0.253
	20	0.385	0.9656	0.399	0.601	−0.509
	30	0.516	0.9656	0.534	0.466	−0.764
	60	0.759	0.9656	0.786	0.214	−1.542
	90	0.874	0.9656	0.905	0.095	−2.355
	120	0.929	0.9656	0.962	0.038	−3.273
	150	0.934	0.9656	0.967	0.033	−3.420

Table 21. Summary of overall and stage-specific effective diffusivity and characteristic diffusion time for NH_4^+ adsorption onto corn-husk particles.

PARTICLE SIZE (μm)	PARAMETER	SLOPE (1/min)	INTERCEPT	D_e (×10^{-13} m^2/s)	τ_d (min)
105	$D_{e,O}$	−0.05410	−0.01348	2.52	182.4
	$D_{e,W}$	−0.05369	−0.04923	2.50	183.8
	$D_{e,N}$	−0.05468	−0.00816	2.55	180.5
250	$D_{e,O}$	−0.03633	−0.05481	9.59	271.7
	$D_{e,W}$	−0.03861	0.01753	10.19	255.6
	$D_{e,N}$	−0.03861	0.01753	10.19	255.6
500	$D_{e,O}$	−0.02455	−0.03691	25.92	401.9
	$D_{e,W}$	−0.02651	0.03696	27.98	372.3
	$D_{e,N}$	−0.02779	0.10077	29.33	355.2

3.7. Scope and Limitations of the Present Study

This study focuses on calculating and interpreting adsorption kinetics, mass-transfer behavior, mechanistic classification, and effective diffusivity using an illustrative batch adsorption system (**Figure 19**). However, adsorption isotherms, thermodynamics, detailed adsorbent characterization, regeneration, fixed-bed operation, and multicomponent adsorption are beyond the present scope. The interpretations rely on mathematical assumptions and illustrative data rather than comprehensive experimental validation.

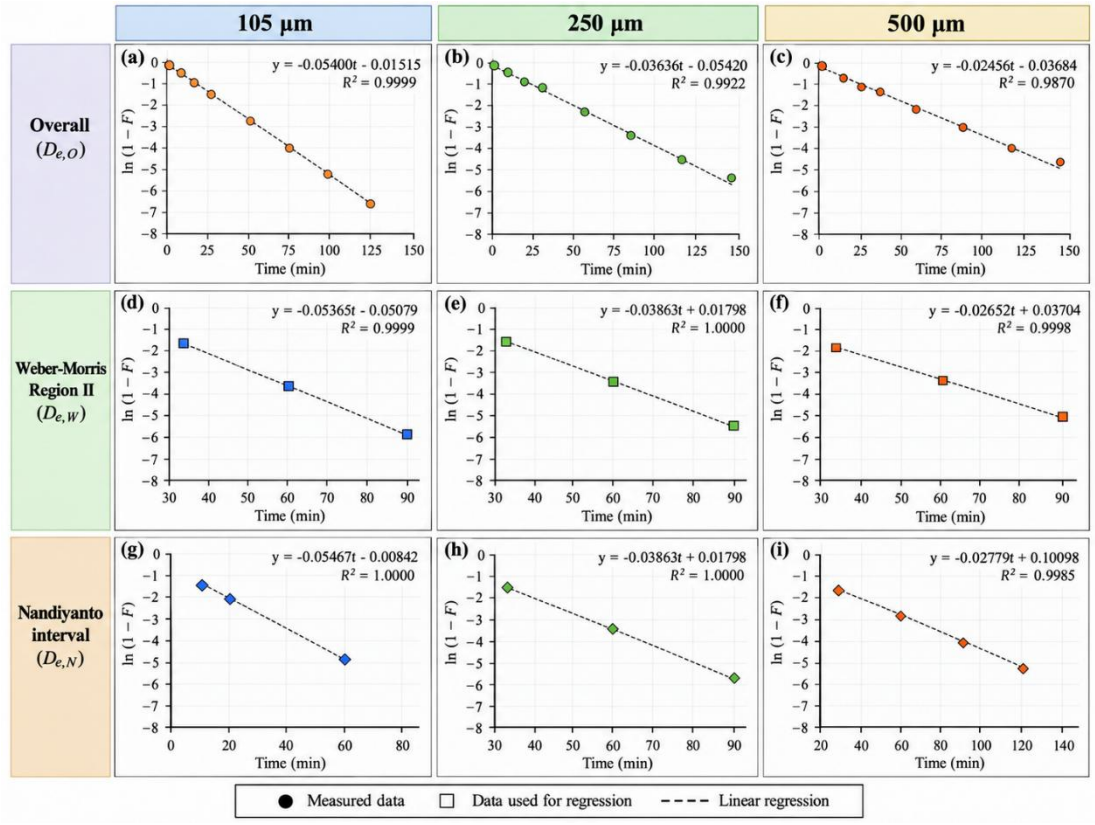


Figure 19. Linearized effective diffusivity analysis for adsorption onto corn-husk at C_0=10 mg/L: (a-c) overall adsorption-based regressions for 105-, 250-, and 500-µm particles; (d-f) regressions using Weber-Morris Region II; and (g-i) regressions using the Nandiyanto intermediate adsorption stage.

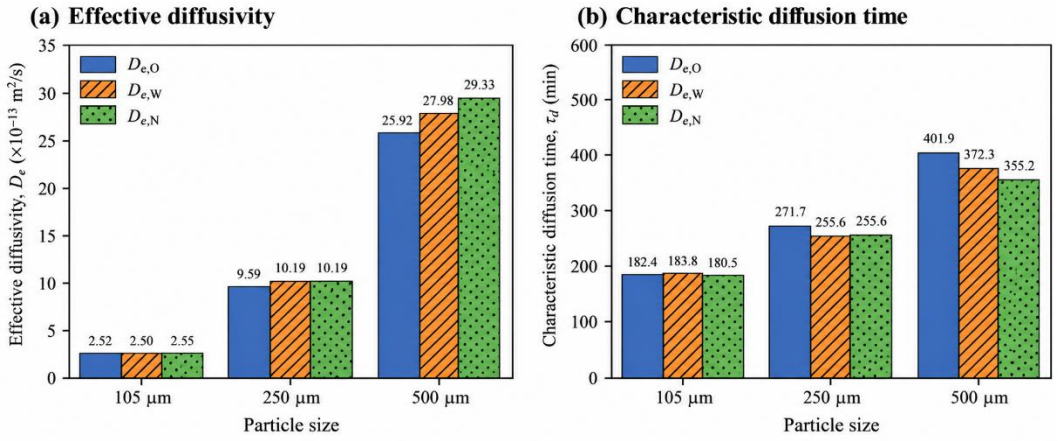


Figure 20. Comparison of (a) apparent effective diffusivity (D_e) and (b) characteristic diffusion time (τ_d) for NH_4^+ adsorption onto corn-husk with particle sizes of 105, 250, and 500 µm. The three approaches represent overall adsorption behavior ($D_{e,O}$), Weber-Morris Region II ($D_{e,W}$), and the intermediate stage of the Nandiyanto classification ($D_{e,N}$).

4. CONCLUSION

This study presents an integrated framework for calculating and interpreting adsorption mass transfer through kinetic, Weber-Morris, Boyd, Fulazzaky, Nandiyanto, Furusawa-Smith, and effective diffusivity analyses. Using NH_4^+ adsorption onto corn-husk particles as a

practical example, the framework demonstrates how particle size influences adsorption behavior and characteristic transport timescales. Smaller particles exhibited faster adsorption progression, whereas larger particles required longer diffusion times. Selecting different adsorption intervals affects calculated mass-transfer parameters. The framework provides a systematic approach for evaluating adsorption kinetics, distinguishing transport stages, and interpreting mass-transfer mechanisms while recognizing model-dependent assumptions.

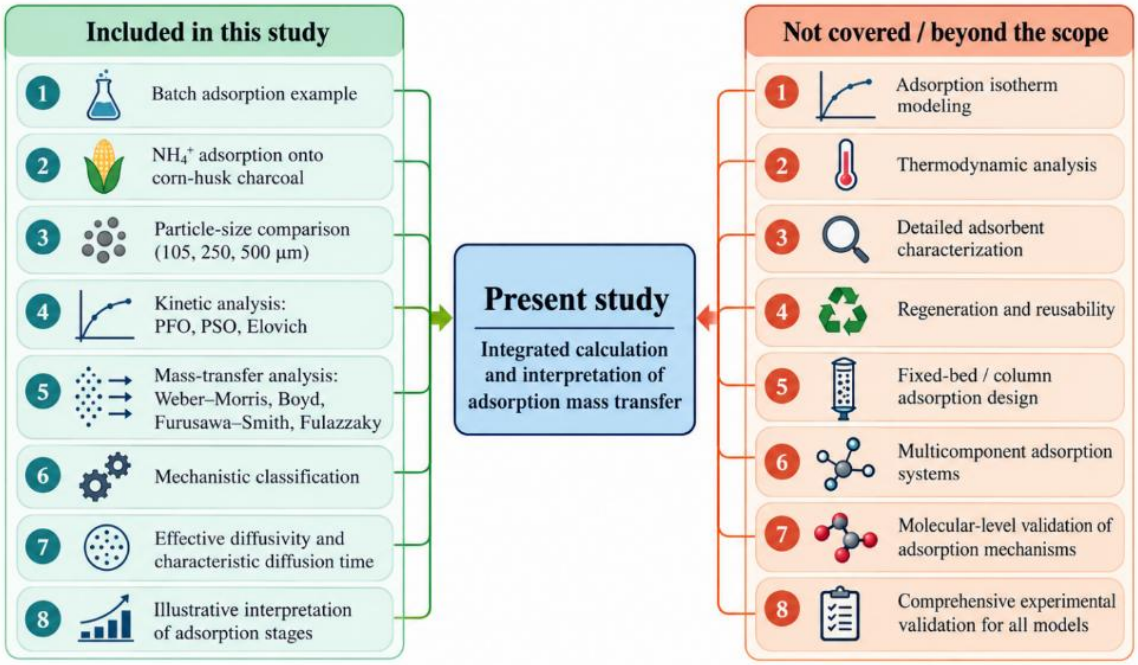


Figure 21. Scope and limitations of the present study.

5. AUTHORS' NOTE

The authors declare that there is no conflict of interest regarding the publication of this article. The authors confirmed that the paper was free of plagiarism.

6. REFERENCES

[1] Revellame, E. D., Fortela, D. L., Sharp, W., Hernandez, R., and Zappi, M. E. (2020). Adsorption kinetic modeling using pseudo-first order and pseudo-second order rate laws: A review. *Cleaner Engineering and Technology*, *1*, 100032.

[2] Ho, Y. S., and McKay, G. (1999). Pseudo-second order model for sorption processes. *Process Biochemistry*, *34*(5), 451-465.

[3] Weber Jr, W. J., and Morris, J. C. (1963). Kinetics of adsorption on carbon from solution. *Journal of the Sanitary Engineering Division*, *89*(2), 31-59.

[4] Boyd, G. E., Adamson, A. W., and Myers Jr, L. S. (1947). The exchange adsorption of ions from aqueous solutions by organic zeolites. II. Kinetics1. *Journal of the American Chemical Society*, *69*(11), 2836-2848.

[5] Lagergren, S. (1898). About the theory of so-called adsorption of soluble substances. *Kungliga Svenska Vetenskapsakademiens Handlingar*, *24*(4), 1-39.

[6] Vareda, J. P. (2023). On validity, physical meaning, mechanism insights and regression of adsorption kinetic models. *Journal of Molecular Liquids*, *376*, 121416.